

# Anisotropic Green Coordinates

DONG XIAO, University of Science and Technology of China, China  
 RENJIE CHEN\*, University of Science and Technology of China, China  
 BAILIN DENG, Cardiff University, UK

We live in a world filled with anisotropy, a ubiquitous characteristic of both natural and engineered systems. In this study, we concentrate on space deformation and introduce *anisotropic Green coordinates*, which provide versatile effects for cage-based and variational deformations in both two and three dimensions. The anisotropic Green coordinates are derived from the anisotropic Laplacian equation  $\nabla \cdot (\mathbf{A}\nabla u) = 0$ , where  $\mathbf{A}$  is a symmetric positive definite matrix. This equation belongs to the class of constant-coefficient second-order elliptic equations, exhibiting properties analogous to the Laplacian equation but incorporating the matrix  $\mathbf{A}$  to characterize anisotropic behavior. Based on this equation, we establish the boundary integral formulation, which is subsequently discretized to derive anisotropic Green coordinates defined on the vertices and normals of oriented simplicial cages. The deformation satisfies basic properties such as linear reproduction and translation invariance, and has closed-form expressions for both 2D and 3D scenarios. We also offer intuitive geometric interpretations of this method. Furthermore, our approach computes the gradient and Hessian of the deformation coordinates and employs the local-global optimization framework to facilitate variational shape deformation, enabling flexible shape manipulation while achieving as-rigid-as-possible shape deformation. Experimental results demonstrate that anisotropic Green coordinates offer versatile and diverse deformation options, providing artists with enhanced flexibility and introducing a novel perspective on spatial deformation.

CCS Concepts: • **Computing methodologies** → **Shape modeling; Geometric deformation.**

Additional Key Words and Phrases: Anisotropic deformation, Green coordinates, Cage-based deformation, Variational shape deformation

## 1 Introduction

Space deformation is a basic problem in geometric modeling. Instead of directly modifying the object surface, space deformation treats the surface as an embedding in the ambient space and deforms the space through deformation handles [Ben-Chen et al. 2009]. Cage-based deformation is a typical example in which the embedded object deforms according to the manipulation of the source cage to the target cage. For each point  $\eta$  within the cage, a series of functions  $\phi_i(\eta)$  is constructed for each cage vertex  $\mathbf{v}_i$ . These functions satisfy the partition of unity property,  $\sum_{i=1}^n \phi_i(\eta) = 1$ , and the linear reproduction property  $\eta = \sum_{i=1}^n \phi_i(\eta)\mathbf{v}_i$ . The functions  $\phi_i(\eta)$  are always called the Generalized Barycentric Coordinates (GBC) [Floater 2015; Hormann and Sukumar 2017].

GBC is usually interpolatory and expresses the point inside the cage as an affine sum of the cage vertices. Although it demonstrates good consistency with the target cage, it introduces obvious shearing artifacts, particularly when the cage undergoes affine transformations [Lipman et al. 2008]. In practice, it is also desirable for the

deformed object to maintain a certain degree of conformality with the original object. Harmonic functions often provide a solution to this issue, as harmonicity is inherently associated with shape preservation. Based on the Green’s third identity of harmonic functions, Lipman et al. [2008] propose Green coordinates, which take into account both the cage vertices  $\mathbf{v}_i$  and the cage normals  $\mathbf{n}_j$ . Green coordinates satisfy  $\eta = \sum_{i=1}^n \phi_i(\eta)\mathbf{v}_i + \sum_{j=1}^m \psi_j(\eta)\mathbf{n}_j$  for  $\eta$  inside the cage. These coordinates enable shape-preserving deformations, characterized by angle-preserving in 2D and quasi-conformality in 3D. However, conformality is a strict and absolute condition. While it provides desirable properties, it also restricts the deformation diversity of Green coordinates once the source and target cages are fixed. In practical applications and artistic design, there is often a demand for more flexible and versatile deformation styles, which can be achieved through adjustments to various parameters. In the real world, materials such as bones, wood, and fibers exhibit anisotropic structures, leading users to desire deformations that are either more “flexible” or more “rigid” along specific directions.

Based on previous observations, our work proposes to introduce the anisotropic property into the traditional Green coordinates. The Laplacian operator is the composition of divergence and gradient, i.e.,  $\Delta = \nabla \cdot \nabla$ . Therefore, we can introduce anisotropy within the divergence operator and consider the anisotropic Laplacian equation  $\nabla \cdot (\mathbf{A}\nabla u) = 0$ , where  $\mathbf{A}$  is a positive-definite matrix. The matrix  $\mathbf{A}$  introduces varying scales in different directions, thereby imparting anisotropic properties in the formulation. Furthermore, the anisotropic Laplacian equation also gives rise to corresponding boundary integral formulation and leads to the anisotropic identity equations, which form the foundation for constructing the anisotropic Green coordinates. We show that anisotropic Green coordinates satisfy linear reproduction and translation invariance properties, and produce versatile deformation results with varying control matrices  $\mathbf{A}$ . Additionally, we provide closed-form expressions for both 2D and 3D cases and offer intuitive geometric interpretations of the method. Through extensive experiments, we validate that anisotropic Green coordinates provide artists with a broader range of deformation options and enhance the diversity of deformations choices. Moreover, appropriate selection of the matrix  $\mathbf{A}$  enables desired effects, such as tighter adherence to the deformed cage or reduced isotropic and area distortion.

To further demonstrate the broad applicability of the closed-form anisotropic Green coordinates, we also compute their gradients and Hessians and perform variational shape deformation [Ben-Chen et al. 2009], which minimizes the energy functional of the deformation map. This approach enables flexible control through positional constraints and supports the as-rigid-as-possible deformation strategy. The incorporation of anisotropy further extends the applicability of the variational shape deformation framework to a wider range of scenarios.

\*Corresponding author

Authors’ Contact Information: Dong Xiao, xiaodong@ustc.edu.cn, School of Mathematical Sciences, University of Science and Technology of China, China; Renjie Chen, renjiecc@ustc.edu.cn, School of Mathematical Sciences, University of Science and Technology of China, China; Bailin Deng, dengb3@cardiff.ac.uk, School of Computer Science and Informatics, Cardiff University, UK.

## 2 Related Work

### 2.1 Cage-based Deformation

Cage-based deformation is a fundamental topic in geometry processing, where users manipulate a coarse control structure to drive the deformation of complex objects within the enclosed space. Two critical factors in this problem are the geometry of the cage structure and the deformation coordinates defined on the cage. The most commonly used cage structure is the oriented simplicial surface, such as closed polygonal chains in 2D and triangle meshes in 3D [Ben-Chen et al. 2009; Ju et al. 2005; Lipman et al. 2008; Thiery et al. 2024; Weber et al. 2012; Yan and Schaefer 2019]. It is the first-order approximation of co-dimensional one surfaces. Other methods utilize high-order surfaces, such as polynomial or Bézier surfaces, as the cage structure [Li et al. 2013; Lin and Chen 2024; Liu et al. 2024a; Michel et al. 2025; Michel and Thiery 2023; Qin et al. 2024; Wu et al. 2025; Xiao and Chen 2025]. Such structures enable more precise and flexible control over curved and bending deformations.

The cage structure mainly influences the flexibility of the deformation; however, the deformation effect is determined by the specific deformation coordinates established on the cage. The most widely utilized methods are generalized barycentric coordinates (GBC), which formulate interpolatory coordinates as a partition of unity and are capable of accurately representing any point  $\eta$  within the cage. As pioneering works, Floater [2003], Floater et al. [2005], and Ju et al. [2005] construct closed-form mean value coordinates by projecting the enclosing cage onto a sphere centered at  $\eta$  and calculating the contribution of each cage vertex based on this spherical projection. There are also other techniques for constructing GBC, such as using the Laplacian equation [Joshi et al. 2007], the Poisson integral formula [Li and Hu 2013], probability theory [Chang et al. 2023; Hormann and Sukumar 2008], or stochastic sampling and Monte Carlo integration [de Goes and Desbrun 2024]. Additionally, transfinite coordinates [Belyaev 2006; Chang and Hormann 2025; Dyken and Floater 2009] extend the concept of traditional discrete barycentric coordinates to continuous boundaries, offering a general theoretical framework.

In addition to barycentric coordinates, some other deformation coordinates consider both the cage vertices and cage normals, and therefore achieve shape-preserving deformations. Shape preservation means that the deformed shape maintains a certain degree of conformality with the original shape and avoids large shearing artifacts. The typical methods are the Green coordinates [Lipman and Levin 2009; Lipman et al. 2008; Thiery and Boubekur 2022; Wu et al. 2025; Xiao and Chen 2025], which utilize Green’s third identity to establish the deformation formulation and naturally satisfy linear reproduction and transformation invariance. Other techniques involve Cauchy coordinates [Lin and Chen 2024; Liu et al. 2024b; Weber et al. 2009], which is demonstrated to be geometrically equivalent to Green coordinates in the planar domain. However, the deformation effects of Green coordinates and Cauchy coordinates are fixed. Specifically, once the source and target cages are determined, the deformation is uniquely defined. To address this limitation, one approach is to solve the biharmonic Dirichlet problem, which incorporates gradient variations into the formulation [Liu et al. 2025; Thiery et al. 2024; Weber et al. 2012]. Alternatively, the variational

deformation technique can be employed to optimize the deformation map, as discussed in the following subsection.

### 2.2 Variational Shape Deformation

Variational methods are widely used in formulating partial differential equations for practical problems, such as the minimal surface equation [Pinkall and Polthier 1993]. They address the most fundamental problem in functional analysis of finding a function  $f$  that minimizes the energy functional  $E(f)$ . Ben-Chen et al. [2009] introduce the variational harmonic map in space deformation, which defines  $E(f)$  based on Green coordinates, enabling deformation control with position constraints and as-rigid-as-possible properties. The optimization problem is solved through a local-global minimization strategy [Liu et al. 2008; Sorkine and Alexa 2007]. This method requires the computation of the Jacobian and Hessian of the Green coordinate. Additionally, some subsequent studies extend variational shape deformation techniques using similar strategies across different coordinate systems and high-order cage structures [Liu et al. 2024b; Michel et al. 2025; Thiery et al. 2024; Weber et al. 2012; Wu et al. 2025]. Furthermore, Dodik et al. [2023] introduce variational barycentric coordinates, a neural field-based framework that optimizes generalized barycentric coordinates while minimizing the total variation.

### 2.3 Anisotropy in Geometry Processing

Anisotropy is a fundamental phenomenon in both natural systems and physical processes, playing an important role in simulating directionally dependent materials and generating adaptive computational domains. Research in this field encompasses theoretical foundations, numerical methodologies, and practical applications.

At the mathematical fundamental level, Owhadi and Zhang [2007] establish a metric-based upscaling framework for elliptic PDEs of the form  $\mathcal{L}u = \nabla \cdot (A(\mathbf{x})\nabla u(\mathbf{x}))$  and rigorously analyze its mathematical properties within the Sobolev space. Kharevych et al. [2009] construct anisotropic elasticity tensors on coarse meshes through harmonic homogenization to preserve fine-scale directional properties. Kim et al. [2019] focus on anisotropic hyperelasticity and propose an anisotropic strain invariant for the inversion-safe energy model, complemented by a rehabilitation technique to address degenerate elements. Lin et al. [2024] derive closed-form expressions for anisotropic invariants, facilitating the stable simulation of directionally dependent materials.

Anisotropy is also well introduced in mesh processing. Chen and Desbrun [2022] expand Green’s functions by leveraging the anisotropic characteristics of general linear elastic materials, which allows for real-time control of material deformation without volumetric discretization. Ren et al. [2018] propose generating planar anisotropic meshes for a given metric tensor and establishing a quasi-conformal mapping to transform the anisotropic metric into a Euclidean metric. Zhong et al. [2013] embed the anisotropic Riemannian metrics into higher-dimensional isotropic spaces, achieving efficient particle-based anisotropic meshing. Ma et al. [2025] derive the anisotropic Gauss formulation and utilize this boundary integral formulation for point cloud normal orientation and surface

reconstruction. This work focuses on geometry topics that are distinct from our method and only considers the anisotropic equations in diagonal forms.

### 3 Anisotropic Green Coordinates

In this section, we present a detailed derivation of the anisotropic Green coordinates. We begin by introducing the boundary integral formulation of the anisotropic Laplacian equation. It is not trivial that, despite the introduction of anisotropy, the equation can still be expressed using boundary integrals to determine the coordinates of any point within the cage. Subsequently, we discretize this integral equation to obtain anisotropic Green coordinates that exhibit linear reproduction and translation invariance. Finally, we analyze their properties.

#### 3.1 Anisotropic Laplacian Equation

Green's third identity can be derived from the Laplacian equation  $\Delta u = 0$ , which serves as the foundation for establishing Green coordinates. Since  $\Delta = \nabla \cdot \nabla$ , we can introduce anisotropy within the divergence operator. Our method starts with the anisotropic Laplacian equation in  $\mathbb{R}^d$ ,  $d \geq 2$ , which is given by:

$$\nabla \cdot (\mathbf{A} \nabla u(\mathbf{x})) = 0, \quad (1)$$

where  $\mathbf{A}$  is a  $d \times d$  positive-definite matrix with constant coefficients. This is the simplification of the second-order elliptic operator  $\mathcal{L}u = \nabla \cdot (\mathbf{A}(\mathbf{x}) \nabla u(\mathbf{x})) + \mathbf{b}(\mathbf{x}) \cdot \nabla u(\mathbf{x}) + cu(\mathbf{x})$  [Evans and Lawrence 1964], which shares similar properties with harmonic functions. When  $\mathbf{A}$  is not a constant matrix, the properties of its solutions are usually analyzed in the Sobolev space. Deriving explicit solutions is often challenging. Thus, we focus on the scenario where  $\mathbf{A}$  is a constant-coefficient matrix, and both the convection-enhancing term  $\mathbf{b}(\mathbf{x})$  and the first-order term  $c$  are set to zero. It has been mathematically established that every differential operator  $L$  with constant coefficients has a fundamental solution [Folland 1995].

We first present a preliminary of the square roots of the positive definite matrix. We know that every positive definite matrix  $\mathbf{A}$  can be expressed as  $\mathbf{A} = \mathbf{P}\mathbf{\Lambda}\mathbf{P}^\top$ , where

$$\mathbf{\Lambda} = \text{diag}(\lambda_1, \lambda_2, \dots, \lambda_d) \quad (2)$$

is a  $d$ -dimensional diagonal matrix, and  $\mathbf{P}$  is an orthogonal matrix satisfying  $\mathbf{P}^{-1} = \mathbf{P}^\top$  [Strang 2003]. By expressing

$$\mathbf{\Lambda}^{1/2} = \text{diag}(\sqrt{\lambda_1}, \sqrt{\lambda_2}, \dots, \sqrt{\lambda_d}), \quad (3)$$

we can define the square root of  $\mathbf{A}$  as  $\mathbf{A}^{1/2} = \mathbf{P}\mathbf{\Lambda}^{1/2}\mathbf{P}^\top$ . It is then straightforward to verify that  $(\mathbf{A}^{1/2})^2 = \mathbf{A}$ .

Next, we will present some theorems related to the anisotropic Laplacian equation. While we believe these properties have been investigated in prior fundamental mathematical research, as they are closely related to the Green's function [Chen and Kuo 2005], we have not identified specific literature in the fields of cage or variational deformation that comprehensively addresses these results. Therefore, we provide a detailed discussion of them in the following.

**THEOREM 1.** *The fundamental solution of the anisotropic Laplacian Equation  $\nabla_\xi \cdot (\mathbf{A} \nabla_\xi G_A(\xi, \eta)) = \delta(\xi - \eta)$  is:*

$$G_A(\xi, \eta) = \begin{cases} \frac{1}{2\pi\sqrt{\det \mathbf{A}}} \log \sqrt{(\xi - \eta)^\top \mathbf{A}^{-1}(\xi - \eta)}, & d = 2, \\ -\frac{1}{(d-2)\omega_d\sqrt{\det \mathbf{A}}} [(\xi - \eta)^\top \mathbf{A}^{-1}(\xi - \eta)]^{\frac{2-d}{2}}, & d \geq 3, \end{cases} \quad (4)$$

where  $\delta(\mathbf{x})$  is the Dirac delta distribution satisfying  $\delta(\mathbf{x}) = 0$  for  $\mathbf{x} \neq \mathbf{0}$  and  $\int_{\mathbb{R}^d} \delta(\mathbf{x}) = 1$ , and  $\omega_d = 2\pi/\Gamma(n/2)$  represents the surface area of the unit sphere in  $\mathbb{R}^d$ .

**PROOF.** Let  $\mathbf{x} = \mathbf{A}^{-1/2}\xi$ ,  $\mathbf{y} = \mathbf{A}^{-1/2}\eta$ . According to lemma A.1 in the supplementary material, and the fact that  $\mathbf{A}^{-1/2}$  is symmetric and invertible, we have  $\nabla_\xi f = \mathbf{A}^{-1/2} \nabla_{\mathbf{x}} f$  and  $\nabla_\xi \cdot \mathbf{F} = \nabla_{\mathbf{x}} \cdot (\mathbf{A}^{-1/2} \mathbf{F})$ , where  $f$  and  $\mathbf{F}$  are scalar and vector value functions. Then,

$$\begin{aligned} \nabla_\xi \cdot (\mathbf{A} \nabla_\xi u) &= \nabla_\xi \cdot (\mathbf{A} \mathbf{A}^{-1/2} \nabla_{\mathbf{x}} u) = \nabla_\xi \cdot (\mathbf{A}^{1/2} \nabla_{\mathbf{x}} u) \\ &= \nabla_{\mathbf{x}} \cdot (\mathbf{A}^{-1/2} \mathbf{A}^{1/2} \nabla_{\mathbf{x}} u) = \Delta_{\mathbf{x}} u. \end{aligned} \quad (5)$$

In the following, we denote by  $G(\mathbf{u}) = G(\mathbf{x}, \mathbf{y})$  the fundamental solution of the isotropic Laplacian equation  $\Delta_{\mathbf{x}} G(\mathbf{x}, \mathbf{y}) = \delta(\mathbf{x} - \mathbf{y})$ , where  $\mathbf{u} = \mathbf{x} - \mathbf{y}$ , and by  $G_A(\xi, \eta)$  the fundamental solution of the anisotropic Laplacian equation  $\nabla_\xi \cdot (\mathbf{A} \nabla_\xi G_A(\xi, \eta)) = \delta(\xi - \eta)$  with respect to  $\mathbf{A}$ . According to Eq. (5), we know that  $G_A$  satisfying

$$\Delta_{\mathbf{x}} G_A(\mathbf{x}, \mathbf{y}) = \delta(\mathbf{A}^{1/2}(\mathbf{x} - \mathbf{y})) = \frac{1}{\sqrt{\det \mathbf{A}}} \delta(\mathbf{x} - \mathbf{y}). \quad (6)$$

For the rightmost equality, refer to Lemma A.2 in the appendix, together with the fact that  $\det \mathbf{A}^{1/2} = |\det \mathbf{A}^{1/2}| = \sqrt{\det \mathbf{A}}$ . Therefore, we conclude that  $\sqrt{\det \mathbf{A}} G_A(\mathbf{x} - \mathbf{y})$  is the fundamental solution  $G(\mathbf{u})$  of  $d$ -dimensional isotropic Laplacian equation, which is given by

$$G(\mathbf{u}) = \begin{cases} \frac{1}{2\pi} \log |\mathbf{u}|, & d = 2, \\ -\frac{1}{(d-2)\omega_d} \frac{1}{|\mathbf{u}|^{d-2}}, & d \geq 3. \end{cases} \quad (7)$$

Substituting  $\mathbf{u} = \mathbf{x} - \mathbf{y} = \mathbf{A}^{-1/2}(\xi - \eta)$  to  $G(\mathbf{u})$  and we complete the proof.  $\square$

Moreover, we can directly compute  $\nabla_\xi G_A(\xi, \eta)$ , which is the gradient of the anisotropic fundamental solution, and it is expressed as follows:

$$\nabla_\xi G_A(\xi, \eta) = \begin{cases} \frac{1}{2\pi\sqrt{\det \mathbf{A}}} [(\xi - \eta)^\top \mathbf{A}^{-1}(\xi - \eta)]^{-1} \mathbf{A}^{-1}(\xi - \eta), & d = 2, \\ \frac{1}{\omega_d\sqrt{\det \mathbf{A}}} [(\xi - \eta)^\top \mathbf{A}^{-1}(\xi - \eta)]^{-\frac{d}{2}} \mathbf{A}^{-1}(\xi - \eta), & d \geq 3. \end{cases} \quad (8)$$

#### 3.2 Construction of Anisotropic Green Coordinates

Before deriving the anisotropic Green coordinates, we first revisit the construction of the classical isotropic Green coordinates, which are defined on an oriented simplicial surface cage  $P = (\mathbb{V}, \mathbb{T})$  [Lipman and Levin 2009; Lipman et al. 2008], where  $\mathbb{V}$  denotes the cage vertices and  $\mathbb{T}$  represents the face normals. Green coordinates are constructed based on Green's third identity. Specifically, when  $\Omega$  is a bounded open set in  $\mathbb{R}^d$  and  $u(\eta)$  is a harmonic function on  $\overline{\Omega}$ , then for  $\eta \in \Omega$ , we have:

$$u(\eta) = \int_{\partial\Omega} u(\xi) \frac{\partial G}{\partial \mathbf{n}_\xi}(\xi, \eta) d\sigma_\xi - \int_{\partial\Omega} G(\xi, \eta) \frac{\partial u}{\partial \mathbf{n}_\xi}(\xi) d\sigma_\xi, \quad (9)$$

where  $G(\xi, \eta)$  is the fundamental solution of the isotropic Laplacian equation (Eq. (7)) with  $\mathbf{u} = \xi - \eta$ .

*Remark:* The left hand side of Eq. (9) can be written as  $c(\eta)u(\eta)$  if  $\eta \in \mathbb{R}^d$  is not constrained in the open set  $\Omega$ . For a smooth boundary  $\Omega$ , the coefficient  $c(\eta)$  satisfies  $c(\eta) = 1$  if  $\eta \in \Omega$ ,  $c(\eta) = 1/2$  if  $\eta \in \partial\Omega$ , and  $c(\eta) = 0$  if  $\eta \in \mathbb{R}^d \setminus \bar{\Omega}$ .

Given the cage  $P = (\mathbb{V}, \mathbb{T})$ , we can use above identity to reproduce any point  $\eta$  inside the cage using the vertices  $\{\mathbf{v}_i | i \in I_V\}$  and normals  $\{\mathbf{n}(t_j) | j \in I_T\}$  of the cage boundary as follows:

$$\eta = F(\eta, P) = \sum_{i \in I_V} \phi_i(\eta) \mathbf{v}_i + \sum_{j \in I_T} \psi_j(\eta) \mathbf{n}(t_j), \quad \eta \in \Omega, \quad (10)$$

where

$$\phi_i(\eta) = \int_{\xi \in N\{\mathbf{v}_i\}} \Gamma_{\mathbf{v}_i}(\xi) \frac{\partial G(\xi, \eta)}{\partial \mathbf{n}(\xi)} d\sigma_\xi, \quad i \in I_V, \quad (11)$$

$$\psi_j(\eta) = - \int_{\xi \in t_j} G(\xi, \eta) d\sigma_\xi, \quad j \in I_T. \quad (12)$$

Here,  $N\{\mathbf{v}_i\}$  represents the faces adjacent to  $\mathbf{v}_i$ , and  $\Gamma_{\mathbf{v}_i}(\xi)$  is a

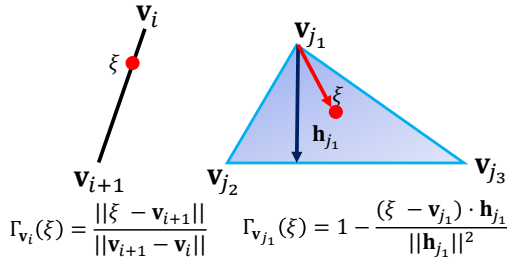


Fig. 1. Illustration of the hat function.

piecewise linear hat function, which takes the value one at the vertex  $\mathbf{v}_i$ , zero at other vertices, and varies linearly on each face adjacent to  $\mathbf{v}_i$ . As shown in Fig. 1, in the 2D case,  $\Gamma_{\mathbf{v}_i}(\xi)$  is given by  $\Gamma_{\mathbf{v}_i}(\xi) = \frac{\|\xi - \mathbf{v}_{i+1}\|}{\|\mathbf{v}_{i+1} - \mathbf{v}_i\|}$ . In the 3D scenario,  $\Gamma_{\mathbf{v}_{j_1}}(\xi)$  is expressed as  $\Gamma_{\mathbf{v}_{j_1}}(\xi) = 1 - \frac{(\xi - \mathbf{v}_{j_1}) \cdot \mathbf{h}_{j_1}}{\|\mathbf{h}_{j_1}\|^2}$ , where  $\mathbf{h}_{j_1}$  is the height of the opposite edge of  $\mathbf{v}_{j_1}$ . Moreover, based on the area ratio,  $\Gamma_{\mathbf{v}_{j_1}}(\xi)$  essentially represents the barycentric coordinate of  $\xi$  relative to  $\mathbf{v}_{j_1}$  within the triangle  $\Delta \mathbf{v}_{j_1} \mathbf{v}_{j_2} \mathbf{v}_{j_3}$ . Therefore,  $\xi = \Gamma_{\mathbf{v}_{j_1}}(\xi) \mathbf{v}_{j_1} + \Gamma_{\mathbf{v}_{j_2}}(\xi) \mathbf{v}_{j_2} + \Gamma_{\mathbf{v}_{j_3}}(\xi) \mathbf{v}_{j_3}$  and  $\Gamma_{\mathbf{v}_{j_1}}(\xi) + \Gamma_{\mathbf{v}_{j_2}}(\xi) + \Gamma_{\mathbf{v}_{j_3}}(\xi) = 1.0$ .

When the source cage  $P$  is deformed to the target cage  $\tilde{P}$ , the new location  $\tilde{\eta}$  toward  $\eta$  is given by

$$\tilde{\eta} = F(\eta, \tilde{P}) = \sum_{i \in I_V} \phi_i(\eta) \tilde{\mathbf{v}}_i + \sum_{j \in I_T} \psi_j(\eta) s_j \tilde{\mathbf{n}}(t_j), \quad (13)$$

where  $\tilde{\mathbf{v}}_i$  and  $\tilde{\mathbf{n}}(t_j)$  are the vertices and normals of the deformed cage, respectively. In the following context, the tilde symbol will consistently be used to represent quantities associated with the deformed value or target cage.  $s_j$  is the scale factor to keep scale invariance in 2D and quasiconformality in 3D, which is detailed in Section 3 of [Lipman et al. 2008].

Next, we derive the anisotropic boundary integral formulation of the anisotropic Laplacian equation, which establishes the mathematical foundation for anisotropic Green coordinates.

**THEOREM 2.** *If  $\Omega$  is a bounded open set in  $\mathbb{R}^d$ , and  $u(\xi)$  is a scalar function satisfying  $\nabla \cdot (\mathbf{A} \nabla u(\xi)) = 0$  on  $\bar{\Omega}$ , where  $\mathbf{A}$  is symmetric positive definite. Then, for  $\eta \in \Omega$ ,*

$$u(\eta) = \int_{\partial\Omega} u(\xi) (\mathbf{A} \nabla G_A(\xi, \eta) \cdot \mathbf{n}(\xi)) d\sigma_\xi - \int_{\partial\Omega} G_A(\xi, \eta) (\mathbf{A} \nabla u(\xi) \cdot \mathbf{n}(\xi)) d\sigma_\xi, \quad (14)$$

where  $G_A(\xi, \eta)$  is the fundamental solution of anisotropic Laplacian equation  $\nabla_\xi \cdot (\mathbf{A} \nabla_\xi G_A(\xi, \eta)) = \delta(\xi - \eta)$ .

**PROOF.** We begin the proof by applying the divergence theorem. Let  $\Omega$  be a bounded open set in  $\mathbb{R}^d$  and  $\mathbf{F}$  is a smooth vector-valued function defined on the closure  $\bar{\Omega}$ . Then,

$$\int_{\Omega} \nabla \cdot \mathbf{F} dV = \int_{\partial\Omega} \mathbf{F} \cdot \mathbf{n} d\sigma, \quad (15)$$

where  $\mathbf{n}$  is the normal vector of  $\partial\Omega$ . Let  $\mathbf{F} = u(\mathbf{A} \nabla v)$ , where  $u, v$  are two scalar functions on  $\bar{\Omega}$ . By applying the rule for computing the divergence of function products, we obtain the following equation:

$$\nabla \cdot \mathbf{F} = \nabla u \cdot (\mathbf{A} \nabla v) + u \nabla \cdot (\mathbf{A} \nabla v). \quad (16)$$

Combining Eqs. (15) and (16), we get

$$\int_{\Omega} \nabla u \cdot (\mathbf{A} \nabla v) + u \nabla \cdot (\mathbf{A} \nabla v) dV = \int_{\partial\Omega} u (\mathbf{A} \nabla v \cdot \mathbf{n}) d\sigma. \quad (17)$$

Exchanging  $u$  and  $v$  in the above equation and obtain

$$\int_{\Omega} \nabla v \cdot (\mathbf{A} \nabla u) + v \nabla \cdot (\mathbf{A} \nabla u) dV = \int_{\partial\Omega} v (\mathbf{A} \nabla u \cdot \mathbf{n}) d\sigma. \quad (18)$$

Then, we can subtract Eq. (18) from Eq. (17). Since  $\mathbf{A}$  is symmetric,

$$\nabla u \cdot (\mathbf{A} \nabla v) = \nabla u^T \mathbf{A} \nabla v = \nabla u^T \mathbf{A}^T \nabla v = (\mathbf{A} \nabla u)^T \nabla v = \nabla v \cdot (\mathbf{A} \nabla u), \quad (19)$$

Therefore, we have

$$\int_{\Omega} u \nabla \cdot (\mathbf{A} \nabla v) - v \nabla \cdot (\mathbf{A} \nabla u) dV = \int_{\partial\Omega} u (\mathbf{A} \nabla v \cdot \mathbf{n}) - v (\mathbf{A} \nabla u \cdot \mathbf{n}) d\sigma. \quad (20)$$

Let  $v(\xi) = G_A(\xi, \eta)$ , where  $\eta \in \Omega$  is fixed, and the integral is taken with respect to the variable  $\xi$ . Then,  $\nabla \cdot (\mathbf{A} \nabla v(\xi)) = \delta(\xi - \eta)$ , and we have

$$\int_{\Omega} u(\xi) \nabla \cdot (\mathbf{A} \nabla G_A(\xi, \eta)) dV_\xi = \int_{\Omega} u(\xi) \delta(\xi - \eta) dV_\xi = u(\eta). \quad (21)$$

Consequently, when  $u$  satisfies  $\nabla \cdot (\mathbf{A} \nabla u(\xi)) = 0$ , we obtain Equation (14) and complete the proof.  $\square$

We can derive the anisotropic Green coordinates with the natural linear reproduction property by utilizing Eq. (14). By setting  $u(\eta) = \eta$ , we can express  $\eta \in \Omega$  in terms of the anisotropic boundary integration. There is a remark that  $u$  is a scalar function in Eq. (14). However, we can separately apply the identity to each component along the coordinate axes. Specifically, let  $u_k(\eta) = \eta_k$ , which returns the  $k$ -th component of  $\eta = (\eta_1, \eta_2, \dots, \eta_d)^T$ . Moreover, let  $\mathbf{A} = (\mathbf{a}_1, \mathbf{a}_2, \dots, \mathbf{a}_d)$ , where  $\mathbf{a}_k$  is the  $k$ -th column of  $\mathbf{A}$ . Then,  $\mathbf{A} \nabla u_k(\xi) \cdot \mathbf{n}(\xi) = (\mathbf{a}_k)^T \mathbf{n}(\xi)$ . We can then combine the  $d$  components to obtain  $\eta = (u_1(\eta), \dots, u_d(\eta))^T$ . Moreover, the composed

normal term on the right-hand side is  $\mathbf{A}^\top \mathbf{n}(t_j) = \mathbf{A}\mathbf{n}(t_j)$ . Considering the boundary integration region as the cage boundary, we have the following equations:

$$\begin{aligned} \eta &= \sum_{j \in I_T} \left( \int_{t_j} \xi (\mathbf{A}\nabla G_A(\xi, \eta) \cdot \mathbf{n}(\xi)) d\sigma_\xi - \int_{t_j} G_A(\xi, \eta) \mathbf{A}\mathbf{n}(\xi) d\sigma_\xi \right) \\ &= \sum_{j \in I_T} \sum_{\mathbf{v}_i \in \mathcal{V}(t_j)} \mathbf{v}_i \left( \int_{t_j} \Gamma_i(\xi) \mathbf{A}\nabla G_A(\xi, \eta) \cdot \mathbf{n}(\xi) d\sigma_\xi \right) \\ &\quad - \sum_{j \in I_T} \mathbf{A}\mathbf{n}(t_j) \left( \int_{t_j} G_A(\xi, \eta) d\sigma_\xi \right), \end{aligned} \quad (22)$$

where  $I_T$  represents the index set of the cage faces. By rearranging the above equation, the anisotropic Green coordinates can be written as:

$$\eta = \sum_{i \in I_V} \phi_i^A(\eta) \mathbf{v}_i + \sum_{j \in I_T} \psi_j^A(\eta) \mathbf{A}\mathbf{n}(t_j), \quad \eta \in \Omega, \quad (23)$$

where

$$\phi_i^A(\eta) = \int_{\xi \in \mathcal{N}\{\mathbf{v}_i\}} \Gamma_i(\xi) \mathbf{A}\nabla G_A(\xi, \eta) \cdot \mathbf{n}(\xi) d\sigma_\xi, \quad i \in I_V, \quad (24)$$

$$\psi_j^A(\eta) = - \int_{\xi \in t_j} G_A(\xi, \eta) d\sigma_\xi, \quad j \in I_T. \quad (25)$$

Compared to the traditional Green coordinates, the integral expressions of  $\phi_i^A(\eta)$  and  $\psi_j^A(\eta)$  are now related to  $G_A(\xi, \eta)$  instead of  $G(\xi, \eta)$ . Moreover, the Neumann term of Eq. (23), which is constructed based on the cage normals, now becomes  $\mathbf{A}\mathbf{n}(t_j)$ . When the source cage is deformed to  $\tilde{P}$  with new vertices  $\tilde{\mathbf{v}}_i$  and face normals  $\tilde{\mathbf{n}}(t_j)$ , the deformed position of  $\eta$  is

$$\tilde{\eta} = \sum_{i \in I_V} \phi_i^A(\eta) \tilde{\mathbf{v}}_i + \sum_{j \in I_T} \psi_j^A(\eta) s_j \tilde{\mathbf{A}}\tilde{\mathbf{n}}(t_j), \quad (26)$$

where  $s_j$  is the scale factor analogous to that in [Lipman et al. 2008]. A detailed discussion of this term will be provided in the following subsection.

### 3.3 Properties

To analyze the deformation properties of the anisotropic Green coordinates (Eq. (26)), we first revisit the properties of the isotropic case, as examined in [Lipman and Levin 2009; Lipman et al. 2008]. Specifically, these properties include: (1) Linear reproduction:  $\eta = F(P, \eta)$  for  $\eta \in \Omega$ ; (2) Translation invariance:  $\sum_{i \in I_V} \phi_i(\eta) = 1$  for  $\eta \in \Omega$ ; (3) Rotation and scale invariance: for an affine transformation  $T$ ,  $T\eta = F(\eta, TP)$ ; (4) Shape preservation: the deformation is angle-preserving in 2D and quasi-conformal in 3D; and (5) Smoothness:  $\phi_i(\eta)$  and  $\psi_j(\eta)$  are  $C^\infty$  for  $\eta \in \Omega$ . We observe that the anisotropic Green coordinates retain the properties of linear reproduction, translation invariance, and scale invariance. However, when  $\mathbf{A} \neq \mathbf{I}$ , it does not satisfy the rotation invariance. Additionally, they are not angle-preserving in 2D.

**Linear reproduction:** The linear reproduction property is directly achieved through the anisotropic boundary integral formula. In Eq. (26), when the source and target cages are identical and  $s_j = 1$ , substituting the coordinate expressions back yields Eq. (22), thereby confirming that  $\tilde{\eta} = \eta$ .

**Translation invariance:** Translation invariance is obtained from the fact that  $\phi_i^A(\eta)$  satisfies the partition of unity, i.e.,  $\sum_{i \in I_V} \phi_i^A(\eta) = 1$ . This can be proven by setting  $u(\eta) = 1$  in Eq. (14). Then, we get

$$\int_{\partial\Omega} (\mathbf{A}\nabla G_A(\xi, \eta) \cdot \mathbf{n}(\xi)) d\sigma_\xi = 1, \quad \eta \in \Omega. \quad (27)$$

Additionally,  $\Gamma_i(\eta)$  in  $\phi_i^A(\eta)$  is actually the barycentric coordinates of the simplices associated with vertices  $\mathbf{v}_i$ . Therefore,

$$\begin{aligned} \sum_{i \in I_V} \phi_i^A(\eta) &= \sum_{j \in I_T} \sum_{\mathbf{v}_i \in \mathcal{V}(t_j)} \left( \int_{t_j} \Gamma_{\mathbf{v}_i}(\xi) (\mathbf{A}\nabla G_A(\xi, \eta) \cdot \mathbf{n}(\xi)) d\sigma_\xi \right) \\ &= \int_{\partial\Omega} (\mathbf{A}\nabla G_A(\xi, \eta) \cdot \mathbf{n}(\xi)) d\sigma_\xi = 1. \end{aligned} \quad (28)$$

**Scale invariance** Anisotropic Green coordinates do not necessarily satisfy rotation invariance, as for any rotation matrix  $\mathbf{T}$ ,  $\mathbf{T}$  and  $\mathbf{A}$  are not necessarily commutative. Regarding the selection of the scaling factor  $s_j$  in Eq (26) for scale invariance, Green coordinates [Lipman et al. 2008] establish a simplex  $S_j$  formed by  $\mathbf{v}_{j_1}$  and  $\mathbf{n}(t_j)$ , and  $\tilde{S}_j$  formed by  $\tilde{\mathbf{v}}_{j_1}$  and  $\tilde{\mathbf{n}}(t_j)$ . They analyze the scaling factor in terms of the stretch of the face to ensure that  $T(S_j)$  is similar to  $\tilde{S}_j$ , concluding that  $s_j = \|T\|_2$ , where  $T$  represents the scale transformation. In the anisotropic case, the simplex is formed by  $\mathbf{v}_{j_1}$  and  $\mathbf{A}\mathbf{n}(t_j)$ , as well as  $\tilde{\mathbf{v}}_{j_1}$  and  $s_j \tilde{\mathbf{A}}\tilde{\mathbf{n}}(t_j)$ , respectively. To ensure that  $T(S_j)$  is similar to  $\tilde{S}_j$ , we can similarly conclude that  $s_j = \|T\|_2$ . Therefore, we adopt a similar approach to Lipman et al. [2008], specifically: In the 2D case,  $s_j$  is defined as the ratio of the length of the deformed edge to that of the original edge, i.e.,  $s_j = \|\tilde{t}_j\|/\|t_j\|$ . In the 3D scenario, the scaling factor is defined as follows:

$$s_j = \frac{\sqrt{\|\tilde{u}\|^2\|v\|^2 - 2(\tilde{u} \cdot \tilde{v}) + \|\tilde{v}\|^2\|u\|^2}}{\sqrt{8\text{area}(t_j)}}, \quad (29)$$

where  $u, v$  and  $\tilde{u}, \tilde{v}$  are two pairs of the corresponding vectors of the triangle  $t_j$  in the source and target cages, respectively.

**Smoothness and generalized harmonic** We also have the property that  $\phi_i^A(\eta)$  and  $\psi_j^A(\eta)$  are smooth for  $\eta \in \Omega$ . The reason is that  $G_A(\xi, \eta)$  is an elementary function with respect to  $\eta$  and has no singularities within the integration domain, given that  $\xi \neq \eta$ . Consequently,  $\phi_i^A(\eta)$  and  $\psi_j^A(\eta)$  are also smooth with respect to  $\eta$ , as they are obtained through differentiation and integration of  $G_A(\xi, \eta)$  (Note that  $\Gamma_i(\xi)$  is independent of  $\eta$ ). We also have  $\nabla_\eta \cdot (\mathbf{A}\nabla_\eta \phi_i^A(\eta)) = 0$  and  $\nabla_\eta \cdot (\mathbf{A}\nabla_\eta \psi_j^A(\eta)) = 0$ . We call this property **generalized harmonic with respect to  $\mathbf{A}$** . This can be briefly proven as follows: Due to the smoothness of  $G_A(\xi, \eta)$  when  $\xi \neq \eta$ , differentiation with respect to  $\eta$  can be interchanged with the integration with respect to  $\xi$ . Moreover, the gradient of  $G_A(\xi, \eta)$  with respect to  $\eta$  is simply the negative of its gradient with respect to  $\xi$ . Given that  $G_A(\xi, \eta)$  is generalized harmonic with respect to  $\mathbf{A}$  in  $\xi$ , it follows that it is also generalized harmonic in  $\eta$  in  $\Omega$ . It follows that  $\phi_i^A(\eta)$  and  $\psi_j^A(\eta)$  also inherit this property.

## 4 Derivation of Closed-form Anisotropic Green Coordinates

In previous sections, we derived the deformation formula for anisotropic Green coordinates and obtained the integral expressions for  $\phi_i^A(\eta)$

and  $\psi_j^A(\eta)$  in Eqs. (24) and (25), respectively. Additionally, we explored several properties associated with this deformation. In this section, we derive the closed-form expressions for  $\phi_i^A(\eta)$  and  $\psi_j^A(\eta)$  in both 2D and 3D scenarios. These analytical solutions are more accurate and computationally efficient compared to numerical methods for evaluating the integrals. In the following derivations, we frequently use formulations for the substitution of area elements on the level-set manifold within embedded simplices. These formulations are provided as Lemmas A.3, A.4, and A.5 in the supplementary materials. Although these lemmas do not rely on advanced mathematical concepts, they are not entirely trivial or immediately obvious. For this reason, detailed proofs are also included in the supplementary materials. Moreover, in Section B of the supplementary material, we provide a detailed derivation of the closed-form expressions for isotropic Green coordinates, including their gradients and Hessians, which form the basis for the anisotropic formulation.

#### 4.1 Closed-form Expressions for 2D Scenario

With the above lemmas, we can now derive the closed-form expressions for the Dirichlet term  $\phi_i^A(\eta)$  and Neumann term  $\psi_j^A(\eta)$  of the anisotropic Green coordinates. We begin by presenting the method in 2D. We assume that the 2D cage is a closed and oriented 1-manifold in  $\mathbb{R}^2$  with vertices  $I_V = \{\mathbf{v}_i\}_{i=1}^N$  and faces  $I_T = \{f_j | f_j = \overrightarrow{\mathbf{v}_j \mathbf{v}_{j+1}}\}$  arranged in counter-clockwise order. We denote  $\mathbf{a}_j = \mathbf{v}_{j+1} - \mathbf{v}_j$ . Then, the outer normal vector  $\mathbf{n}_j$  of  $f_j$  is then given by  $\mathbf{n}_j = \mathbf{a}_j^\perp / \|\mathbf{a}_j^\perp\|$ , where the superscript “ $\perp$ ” denotes the vector obtained by rotating the original vector 90 degrees clockwise. Then,  $\psi_j^A(\eta)$  has the following expression:

$$\psi_j^A(\eta) = - \int_{\xi \in f_j} G_A(\xi, \eta) d\sigma_\xi, \quad (30)$$

$$= \int_{\xi \in f_j} -\frac{1}{2\pi \sqrt{\det \mathbf{A}}} \log \sqrt{(\xi - \eta)^\top \mathbf{A}^{-1} (\xi - \eta)} d\sigma_\xi. \quad (31)$$

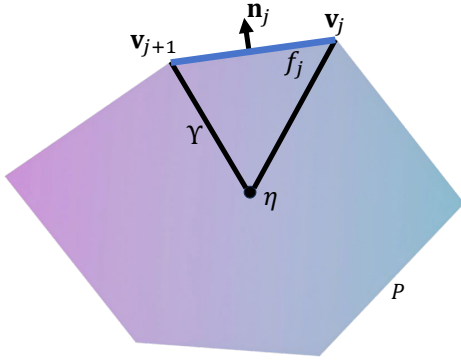


Fig. 2. The illustration of a 2D cage and its mathematical notations.

The key step is to transform the anisotropic calculation into the isotropic one through a variable substitution. Let  $\mathbf{x} = \mathbf{A}^{-1/2} \xi$ ,  $\mathbf{y} = \mathbf{A}^{-1/2} \eta$ ,  $\mathbf{v}'_j = \mathbf{A}^{-1/2} \mathbf{v}_j$  and  $\mathbf{v}'_{j+1} = \mathbf{A}^{-1/2} \mathbf{v}_{j+1}$ . According to Lemma A.3 and Lemma A.4 of the supplementary material, we have  $d\sigma_{\mathbf{x}} =$

$|\det \mathbf{A}^{-1/2}| \|\mathbf{A}^{1/2} \mathbf{n}_j\| d\sigma_\xi$ , where  $\mathbf{n}_j$  is the unit normal of  $f_j$ . Denote  $f'_j = \overrightarrow{\mathbf{v}'_j \mathbf{v}'_{j+1}}$ , we have

$$\psi_j^A(\eta) = \int_{\xi \in f_j} -\frac{1}{2\pi \sqrt{\det \mathbf{A}}} \log \sqrt{(\xi - \eta)^\top \mathbf{A}^{-1} (\xi - \eta)} d\sigma_\xi \quad (32)$$

$$= \frac{1}{|\det \mathbf{A}^{-1/2}| \|\mathbf{A}^{1/2} \mathbf{n}_j\|} \int_{\xi \in f'_j} -\frac{1}{2\pi \sqrt{\det \mathbf{A}}} \log \|\mathbf{x} - \mathbf{y}\| d\sigma_{\mathbf{x}} \quad (33)$$

$$= \frac{1}{\|\mathbf{n}_j^\top \mathbf{A} \mathbf{n}_j\|} \int_{\xi \in f'_j} -\frac{1}{2\pi} \log \|\mathbf{x} - \mathbf{y}\| d\sigma_{\mathbf{x}}. \quad (34)$$

Then, we transform the calculation of the anisotropic formulation into that of the isotropic one. According to [Lipman and Levin 2009], we can define  $\mathbf{a}_j = \mathbf{v}'_{j+1} - \mathbf{v}'_j$  and  $\mathbf{b}_j = \mathbf{v}'_j - \mathbf{y}$ . Then, the term  $-\int_{\xi \in f'_j} \frac{1}{2\pi} \log \|\mathbf{x} - \mathbf{y}\| d\sigma_{\mathbf{x}}$  is equal to  $-\frac{\|\mathbf{a}_j\|}{4\pi} (Q(1) - Q(0))$ , where

$$Q(t) = \left( t + \frac{\mathbf{a}_j \cdot \mathbf{b}_j}{\|\mathbf{a}_j\|^2} \right) \log (\|\mathbf{a}_j\|^2 t^2 + 2(\mathbf{a}_j \cdot \mathbf{b}_j)t + \|\mathbf{b}_j\|^2) - \left( \frac{\|\mathbf{a}_j\|^2 + (\mathbf{a}_j \cdot \mathbf{b}_j)}{\|\mathbf{a}_j\|^2 \sqrt{\|\mathbf{a}_j\|^2 \|\mathbf{b}_j\|^2 - (\mathbf{a}_j \cdot \mathbf{b}_j)^2}} \right) \arctan \left( \frac{\|\mathbf{a}_j\|^2 t + (\mathbf{a}_j \cdot \mathbf{b}_j)}{\sqrt{\|\mathbf{a}_j\|^2 \|\mathbf{b}_j\|^2 - (\mathbf{a}_j \cdot \mathbf{b}_j)^2}} \right). \quad (35)$$

Next, we describe the calculation of the Dirichlet term  $\phi_{\mathbf{v}_j}^A(\eta)$  for the anisotropic Green coordinates. Since  $\phi_{\mathbf{v}_j}^A(\eta)$  is obtained by summing the integrals over the edges associated with  $\mathbf{v}_i$ , we focus on the integral over a single edge  $f_j$ , which is denoted as  $\phi_{\mathbf{v}_j, f_j}^A(\eta)$ . Recall that  $\mathbf{x} = \mathbf{A}^{-1/2} \xi$ ,  $\mathbf{y} = \mathbf{A}^{-1/2} \eta$ ,  $\mathbf{v}'_j = \mathbf{A}^{-1/2} \mathbf{v}_j$ ,  $\mathbf{v}'_{j+1} = \mathbf{A}^{-1/2} \mathbf{v}_{j+1}$ ,  $f_j = \overrightarrow{\mathbf{v}_j \mathbf{v}_{j+1}}$  and  $f'_j = \overrightarrow{\mathbf{v}'_j \mathbf{v}'_{j+1}}$ . Let  $\Gamma_{\mathbf{v}_j, f_j}(\xi)$  be the hat-function of  $\xi$  toward  $\mathbf{v}_j$  in  $f_j$ , and  $\Gamma_{\mathbf{v}'_j, f'_j}(\mathbf{x})$  be the hat-function of  $\mathbf{x}$  toward  $\mathbf{v}'_j$  in  $f'_j$ . We first show that  $\Gamma_{\mathbf{v}_j, f_j}(\xi_0) = \Gamma_{\mathbf{v}'_j, f'_j}(\mathbf{x}_0)$  for  $\xi_0 \in f_j$  and  $\mathbf{x}_0 = \mathbf{A}^{-1/2} \xi_0$ . First, we have

$$\xi_0 = \Gamma_{\mathbf{v}_j, f_j}(\xi_0) \mathbf{v}_j + \Gamma_{\mathbf{v}_{j+1}, f_j}(\xi_0) \mathbf{v}_{j+1} \quad (36)$$

and

$$\Gamma_{\mathbf{v}_j, f_j}(\xi) + \Gamma_{\mathbf{v}_{j+1}, f_j}(\xi) = 1. \quad (37)$$

Therefore,

$$\begin{aligned} \mathbf{x}_0 &= \mathbf{A}^{-1/2} \xi_0 = \Gamma_{\mathbf{v}_j, f_j}(\xi_0) \mathbf{A}^{-1/2} \mathbf{v}_j + \Gamma_{\mathbf{v}_{j+1}, f_j}(\xi_0) \mathbf{A}^{-1/2} \mathbf{v}_{j+1} \\ &= \Gamma_{\mathbf{v}'_j, f'_j}(\mathbf{x}_0) \mathbf{v}'_j + \Gamma_{\mathbf{v}'_{j+1}, f'_j}(\mathbf{x}_0) \mathbf{v}'_{j+1}. \end{aligned} \quad (38)$$

Therefore,  $\Gamma_{\mathbf{v}_j, f_j}(\xi_0)$ ,  $\Gamma_{\mathbf{v}_{j+1}, f_j}(\xi_0)$  and  $\Gamma_{\mathbf{v}'_j, f'_j}(\mathbf{x}_0)$ ,  $\Gamma_{\mathbf{v}'_{j+1}, f'_j}(\mathbf{x}_0)$  are both barycentric coordinates of  $\mathbf{x}_0$  in  $f'_j$ . As established in Lemma A.6 of the supplementary material, the barycentric coordinates of a simplex are uniquely determined due to the affine independence of its vertices. This property distinguishes them from barycentric coordinates in arbitrary polygonal domains, where uniqueness is not guaranteed. Therefore, we conclude that  $\Gamma_{\mathbf{v}_j, f_j}(\xi_0) = \Gamma_{\mathbf{v}'_j, f'_j}(\mathbf{x}_0)$  for any  $\xi_0 \in f_j$  and  $\mathbf{x}_0 = \mathbf{A}^{-1/2} \xi_0$ . Moreover, we have  $d\sigma_\xi = |\det \mathbf{A}^{1/2}| \|\mathbf{A}^{-1/2} \mathbf{n}'_j\| d\sigma_{\mathbf{x}}$ , where  $\mathbf{n}'_j$  is the unit normal of  $\overrightarrow{\mathbf{v}'_j \mathbf{v}'_{j+1}}$ . Then, we can derive the closed-form solution of  $\phi_{\mathbf{v}_j, f_j}^A(\eta)$  as

follows:

$$\begin{aligned}\phi_{\mathbf{v}_j, f_j}^{\mathbf{A}}(\eta) &= \frac{1}{2\pi\sqrt{\det \mathbf{A}}} \int_{\xi \in f_j} \Gamma_{\mathbf{v}_j, f_j}(\xi) \frac{(\xi - \eta) \cdot \mathbf{n}_j}{(\xi - \eta)^\top \mathbf{A}^{-1}(\xi - \eta)} d\sigma_\xi \\ &= \frac{|\det \mathbf{A}^{1/2}| \|\mathbf{A}^{-1/2} \mathbf{n}'_j\|}{2\pi\sqrt{\det \mathbf{A}}} \int_{\mathbf{x} \in f'_j} \Gamma_{\mathbf{v}'_j, f'_j}(\mathbf{x}) \frac{\mathbf{A}^{1/2}(\mathbf{x} - \mathbf{y}) \cdot (\frac{\mathbf{A}^{-1/2} \mathbf{n}'_j}{\|\mathbf{A}^{-1/2} \mathbf{n}'_j\|})}{(\mathbf{x} - \mathbf{y})^\top (\mathbf{x} - \mathbf{y})} d\mathbf{x} \\ &= \frac{1}{2\pi} \int_{\mathbf{x} \in f'_j} \Gamma_{\mathbf{v}'_j, f'_j}(\mathbf{x}) \frac{(\mathbf{x} - \mathbf{y}) \cdot \mathbf{n}'_j}{(\mathbf{x} - \mathbf{y})^\top (\mathbf{x} - \mathbf{y})} d\mathbf{x}.\end{aligned}\quad (39)$$

Recall that  $\mathbf{a}_j = \mathbf{v}'_{j+1} - \mathbf{v}'_j$  and  $\mathbf{b}_j = \mathbf{v}'_j - \mathbf{y}$ . The term

$$\int_{\mathbf{x} \in f'_j} \Gamma_{\mathbf{v}'_j, f'_j}(\mathbf{x}) \frac{(\mathbf{x} - \mathbf{y}) \cdot \mathbf{n}'_j}{(\mathbf{x} - \mathbf{y})^\top (\mathbf{x} - \mathbf{y})} d\mathbf{x} \quad (40)$$

is equal to  $-\frac{\|\mathbf{a}_j\|(\mathbf{b}_j \cdot \mathbf{n}_j)}{2\pi} (W(1) - W(0))$ , where

$$\begin{aligned}W(t) &= \frac{1}{2\|\mathbf{a}_j\|^2} \log(\|\mathbf{a}_j\|^2 t^2 + 2t(\mathbf{a}_j \cdot \mathbf{b}_j) + \|\mathbf{b}_j\|^2) \\ &\quad - \left( \frac{\|\mathbf{a}_j\|^2 + (\mathbf{a}_j \cdot \mathbf{b}_j)}{\|\mathbf{a}_j\|^2 \sqrt{\|\mathbf{a}_j\|^2 \|\mathbf{b}_j\|^2 - (\mathbf{a}_j \cdot \mathbf{b}_j)^2}} \right) \arctan \left( \frac{\|\mathbf{a}_j\|^2 t + (\mathbf{a}_j \cdot \mathbf{b}_j)}{\sqrt{\|\mathbf{a}_j\|^2 \|\mathbf{b}_j\|^2 - (\mathbf{a}_j \cdot \mathbf{b}_j)^2}} \right).\end{aligned}\quad (41)$$

#### 4.2 Closed-form Expressions for 3D Scenario

We can employ a similar methodology to derive the closed-form expression for anisotropic Green coordinates in three dimensions. Fig. 3 illustrates a tetrahedron formed by a triangular face  $t_j = \Delta \mathbf{v}_{j_1} \mathbf{v}_{j_2} \mathbf{v}_{j_3}$  of the cage and an interior point  $\eta$  located within the cage. Let  $\mathbf{x} = \mathbf{A}^{-1/2} \xi$ ,  $\mathbf{y} = \mathbf{A}^{-1/2} \eta$ ,  $\mathbf{v}'_{j_1} = \mathbf{A}^{-1/2} \mathbf{v}_{j_1}$ ,  $\mathbf{v}'_{j_2} = \mathbf{A}^{-1/2} \mathbf{v}_{j_2}$  and  $\mathbf{v}'_{j_3} = \mathbf{A}^{-1/2} \mathbf{v}_{j_3}$ . Based on Lemma A.5 in the supplementary material, and given that  $\mathbf{A}$  is symmetric, we have  $d\sigma_{\mathbf{x}} = |\det \mathbf{A}^{-1/2}| \|\mathbf{A}^{1/2} \mathbf{n}_t\| d\sigma_\xi$ , where  $\mathbf{n}_t$  represents the unit normal vector of  $t_j$ . Moreover, denoting  $t'_j = \Delta \mathbf{v}'_{j_1} \mathbf{v}'_{j_2} \mathbf{v}'_{j_3}$  with normal  $\mathbf{n}'_t$ . Then, the Neumann term  $\psi_j^{\mathbf{A}}(\eta)$  of  $t_j$  can be computed as:

$$\begin{aligned}\psi_j^{\mathbf{A}}(\eta) &= \int_{\xi \in t_j} \frac{1}{4\pi\sqrt{\det \mathbf{A}}} \frac{1}{(\xi - \eta)^\top \mathbf{A}^{-1}(\xi - \eta)} d\sigma_\xi \\ &= \frac{1}{|\det \mathbf{A}^{-1/2}| \|\mathbf{A}^{1/2} \mathbf{n}_t\|} \int_{\mathbf{x} \in t'_j} \frac{1}{4\pi\sqrt{\det \mathbf{A}}} \frac{1}{\|\mathbf{x} - \mathbf{y}\|} d\sigma_{\mathbf{x}} \quad (42) \\ &= \frac{1}{\sqrt{\mathbf{n}_t^\top \mathbf{A} \mathbf{n}_t}} \int_{\mathbf{x} \in t'_j} \frac{1}{4\pi} \frac{1}{\|\mathbf{x} - \mathbf{y}\|} d\sigma_{\mathbf{x}}.\end{aligned}$$

For the Dirichlet term, we apply  $\phi_{\mathbf{v}_{j_1}, t_j}^{\mathbf{A}}(\eta)$  to denote the contribution of  $t_j$  to  $\phi_{\mathbf{v}_{j_1}}^{\mathbf{A}}(\eta)$ . According to the uniqueness of the barycentric coordinates of a simplex (Lemma A.6), we also have  $\Gamma_{\mathbf{v}_{j_1}, t_j}(\xi_0) = \Gamma_{\mathbf{v}'_{j_1}, t'_j}(\mathbf{x}_0)$  for  $\xi_0 \in t_j$  and  $\mathbf{x}_0 = \mathbf{A}^{-1/2} \xi_0$ . Therefore,

$$\begin{aligned}\phi_{\mathbf{v}_{j_1}, t_j}^{\mathbf{A}}(\eta) &= \frac{1}{4\pi\sqrt{\det \mathbf{A}}} \int_{\xi \in t_j} \Gamma_{\mathbf{v}_{j_1}, t_j}(\xi) \frac{(\xi - \eta) \cdot \mathbf{n}_t}{[(\xi - \eta)^\top \mathbf{A}^{-1}(\xi - \eta)]^{\frac{3}{2}}} d\sigma_\xi \\ &= \frac{|\det \mathbf{A}^{1/2}| \|\mathbf{A}^{-1/2} \mathbf{n}'_t\|}{4\pi\sqrt{\det \mathbf{A}}} \int_{\mathbf{x} \in t'_j} \Gamma_{\mathbf{v}'_{j_1}, t'_j}(\mathbf{x}) \frac{\mathbf{A}^{1/2}(\mathbf{x} - \mathbf{y}) \cdot (\frac{\mathbf{A}^{-1/2} \mathbf{n}'_t}{\|\mathbf{A}^{-1/2} \mathbf{n}'_t\|})}{[(\mathbf{x} - \mathbf{y})^\top (\mathbf{x} - \mathbf{y})]^{\frac{3}{2}}} d\mathbf{x} \\ &= \frac{1}{4\pi} \int_{\mathbf{x} \in t'_j} \Gamma_{\mathbf{v}'_{j_1}, t'_j}(\mathbf{x}) \frac{(\mathbf{x} - \mathbf{y}) \cdot \mathbf{n}'_t}{[(\mathbf{x} - \mathbf{y})^\top (\mathbf{x} - \mathbf{y})]^{\frac{3}{2}}} d\mathbf{x}.\end{aligned}\quad (43)$$

Then, we convert the computation of anisotropic coordinates into isotropic coordinates. The calculation of 3D isotropic Green coordinates is relatively complex, with details provided in Section B.2

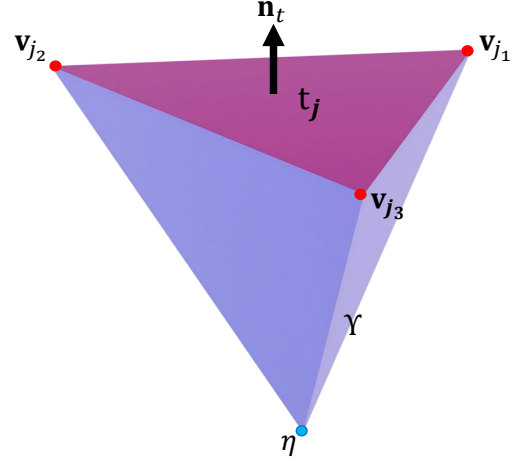


Fig. 3. A tetrahedron formed by a triangular face  $t_j = \Delta \mathbf{v}_{j_1} \mathbf{v}_{j_2} \mathbf{v}_{j_3}$  of a cage and the query point  $\eta$ .

of the supplementary material. The approach is primarily derived from the findings in [Ben-Chen et al. 2009] and [Urago 2000], but we offer a more detailed derivation.

#### 5 Discussion

In the previous section, we derived the expression for anisotropic Green coordinates and obtained their closed-form representation. In this section, we will clarify the geometric interpretation of anisotropic Green coordinates in comparison to the isotropic counterparts and present a proof. Furthermore, we will emphasize the essential value of considering problems from an anisotropic perspective. We have the following observation when ignoring the effect of the scale factor  $s_j$ : the two approaches below are equivalent: 1. Given an input, first multiply the input globally, including the source cage, target cage, and the object, by  $\mathbf{A}^{-1/2}$ , then apply the isotropic deformation, and finally multiply globally by  $\mathbf{A}^{1/2}$ ; 2. Using the anisotropic Green coordinates for the source and target cage. However, we believe that there are still important points to illustrate the value of deriving the anisotropic Green coordinates. First, our method provides a geometric interpretation of the integral formula in terms of the anisotropic Laplacian equation. Second, as deformation coordinates, they need to be expressed as functions relative to the original cage, rather than the cage has undergone a global transformation. Finally, when computing the Jacobian and Hessian of the coordinates, and applying the variational method for deformation control—which will be presented in Section 6—we require the expressions of  $\phi_i^{\mathbf{A}}(\eta)$  and  $\psi_i^{\mathbf{A}}(\eta)$  in terms of the anisotropic Green coordinates.

Next, we refer to the deformation effect obtained by “globally multiplying by  $\mathbf{A}^{-1/2}$ , performing deformation using isotropic Green coordinates, and then globally multiplying by  $\mathbf{A}^{1/2}$ ”, as *similarity Green deformation*. The name stems from the fact that this process closely resembles a matrix similarity transformation. Subsequently, we prove that anisotropic Green deformation is equivalent to similarity Green deformation. We denote the vertices and normals of the source and target cage as  $\{\mathbf{v}_i\}_{i=1}^N$  and  $\{\mathbf{n}_j\}_{j=1}^M$ . Moreover, we use

the prime operator “ $\prime$ ” to denote the globally transformed values, e.g.,  $\mathbf{v}'_i = \mathbf{A}^{-1/2}\mathbf{v}_i$ ,  $\mathbf{n}'_j = \frac{\mathbf{A}^{1/2}\mathbf{n}_j}{\|\mathbf{A}^{1/2}\mathbf{n}_j\|}$ . Then, we can express the globally transformed values in terms of isotropic Green coordinates as:

$$\eta' = \sum_{i \in I_{V'}} \phi'_i(\eta') \mathbf{v}'_i + \sum_{j \in I_{T'}} \psi'_j(\eta') \mathbf{n}'_j. \quad (44)$$

The derivation of section 4.2 shows that  $\phi'_i(\eta') = \phi_i^{\mathbf{A}}(\eta)$  and  $\psi'_j(\eta') = \|\mathbf{A}^{1/2}\mathbf{n}_j\| \psi_j^{\mathbf{A}}(\eta)$ , where  $\mathbf{n}_j$  is the normal of  $f_j$ . Moreover, we have  $\eta = \mathbf{A}^{1/2}\eta'$ . Then,

$$\begin{aligned} \eta &= \mathbf{A}^{1/2}\eta' = \mathbf{A}^{1/2} \left( \sum_{i \in I_{V'}} \phi'_i(\eta') \mathbf{v}'_i + \sum_{j \in I_{T'}} \psi'_j(\eta') \mathbf{n}'_j \right) \\ &= \mathbf{A}^{1/2} \left( \sum_{i \in I_V} \phi_i^{\mathbf{A}}(\eta) \mathbf{A}^{-1/2} \mathbf{v}_i + \|\mathbf{A}^{1/2}\mathbf{n}_j\| \sum_{j \in I_T} \psi_j^{\mathbf{A}}(\eta) \frac{\mathbf{A}^{1/2}\mathbf{n}_j}{\|\mathbf{A}^{1/2}\mathbf{n}_j\|} \right) \\ &= \sum_{i \in I_V} \phi_i^{\mathbf{A}}(\eta) \mathbf{v}_i + \sum_{j \in I_T} \psi_j^{\mathbf{A}}(\eta) \mathbf{A}\mathbf{n}_j, \end{aligned} \quad (45)$$

and we complete the proof of the equivalence between the anisotropic Green deformation and the similarity Green deformation.

## 6 Variational Shape Deformation of Anisotropic Green Coordinates

In Section 4, we derive the closed-form expressions for anisotropic Green coordinates. This section further demonstrates that the gradient and Hessian can also be easily obtained, forming the basis for deformation control in variational shape deformation as introduced in Ben-Chen et al. [2009] and subsequent works such as Michel et al. [2025]; Thiery et al. [2024] and Wu et al. [2025]. Specifically, this method defines an energy functional to determine the optimal deformation mapping that satisfies user-specified constraints while simultaneously balancing as-rigid-as-possible transformation and smoothness.

For a 2D or 3D simplicial surface cage with vertices  $I_V$  and faces  $I_T$ , we can define the deformation map  $f_{\mathbf{a},\mathbf{b}}(\eta)$  as a linear combination of basis functions  $\phi_i^{\mathbf{A}}(\eta)$  and  $\psi_j^{\mathbf{A}}(\eta)$  based on the anisotropic Green coordinates as

$$f_{\mathbf{a},\mathbf{b}}(\eta) = \sum_{v \in I_V} \mathbf{a}_v \phi_v^{\mathbf{A}}(\eta) + \sum_{t \in I_T} \mathbf{b}_t \psi_t^{\mathbf{A}}(\eta), \quad (46)$$

where  $\mathbf{b}_t = \mathbf{A}\mathbf{n}_t$ . Here,  $\mathbf{a}_v$  and  $\mathbf{b}_t$  are treated as independent variables and optimized separately to expand the deformation space. Specifically,  $\mathbf{a}_v \in \mathbb{R}^3$  represents the piecewise-linear coefficients defined on the cage vertices, while  $\mathbf{n}_t \in \mathbb{R}^3$  denotes the piecewise-constant coefficients defined on the cage faces. Since  $\mathbf{A}$  is invertible, we can directly optimize  $\mathbf{b}_t = \mathbf{A}\mathbf{n}_t$ , as  $\mathbf{n}_t$  can be easily computed through  $\mathbf{n}_t = \mathbf{A}^{-1}\mathbf{b}_t$ .

To perform variational shape deformation, we need the gradient and Hessian of  $\phi_i^{\mathbf{A}}(\eta)$  and  $\psi_j^{\mathbf{A}}(\eta)$ . The core idea involves applying Lemma A.1 from the supplementary material to transform the deformation into an isotropic form. For the computation of the gradient and Hessian in isotropic coordinates, refer to Section B of the supplementary material.

Let  $C$  denote the original simplex of a cage, and let  $C'$  represent the transformed simplex obtained by left-multiplying all its vertices by  $\mathbf{A}^{-1/2}$ . Let  $\eta_0$  be a point in  $C$ ,  $\mathbf{n}_j$  the normal of  $C$ , and  $\mathbf{y}_0 = \mathbf{A}^{-1/2}\eta_0$ .

We define  $\psi_j^{\mathbf{A}}(\eta_0, C)$  as the value of the Neumann term in anisotropic coordinates at  $\eta_0$ . Then, based on the derivations in Section 4.2, we obtain:

$$\psi_j^{\mathbf{A}}(\eta_0, C) = \frac{1}{\sqrt{\mathbf{n}_j^{\top} \mathbf{A} \mathbf{n}_j}} \psi_j(\mathbf{y}_0, C'), \quad (47)$$

where  $\psi_j(\mathbf{y}_0, C')$  denotes the corresponding isotropic value. Then, according to Lemma A.1, the gradient  $\nabla_{\eta} \psi_j^{\mathbf{A}}(\eta, C)$  and Hessian  $H_{\eta} \psi_j^{\mathbf{A}}(\eta, C)$  can be calculated as:

$$\begin{aligned} \nabla_{\eta} \psi_j^{\mathbf{A}}(\eta_0, C) &= \frac{1}{\sqrt{\mathbf{n}_j^{\top} \mathbf{A} \mathbf{n}_j}} \mathbf{A}^{-1/2} \nabla_{\mathbf{y}} \psi(\mathbf{y}_0, C'), \\ H_{\eta} \psi_j^{\mathbf{A}}(\eta_0, C) &= \frac{1}{\sqrt{\mathbf{n}_j^{\top} \mathbf{A} \mathbf{n}_j}} \mathbf{A}^{-1/2} H_{\mathbf{y}} \psi(\mathbf{y}_0, C') \mathbf{A}^{-1/2}. \end{aligned} \quad (48)$$

For the Dirichlet term, we denote  $\phi_{i,C}^{\mathbf{A}}(\eta_0, C)$  as the contribution of the integration over  $C$  to  $\phi_i^{\mathbf{A}}(\eta)$ . Based on the derivations in Section 4.2, we have:

$$\phi_{i,C}^{\mathbf{A}}(\eta_0, C) = \phi_{i,C'}(\mathbf{y}_0, C'). \quad (49)$$

Then, the gradient  $\nabla_{\eta} \phi_{i,C}^{\mathbf{A}}(\eta_0, C)$  and Hessian  $H_{\eta} \phi_{i,C}^{\mathbf{A}}(\eta, C)$  can be calculated as:

$$\begin{aligned} \nabla_{\eta} \phi_{i,C}^{\mathbf{A}}(\eta_0, C) &= \mathbf{A}^{-1/2} \nabla_{\mathbf{y}} \phi_{i,C'}(\mathbf{y}_0, C'), \\ H_{\eta} \phi_{i,C}^{\mathbf{A}}(\eta_0, C) &= \mathbf{A}^{-1/2} H_{\mathbf{y}} \phi_{i,C'}(\mathbf{y}_0, C') \mathbf{A}^{-1/2}. \end{aligned} \quad (50)$$

The computation of  $\nabla_{\mathbf{y}} \psi(\mathbf{y}_0, C')$ ,  $H_{\eta} \psi_j^{\mathbf{A}}(\eta, C)$ ,  $\nabla_{\mathbf{y}} \phi_{i,C'}(\mathbf{y}_0, C')$  and  $H_{\mathbf{y}} \phi_{i,C'}(\mathbf{y}_0, C')$  can be found in Section B.2.

Next, we return to the formulation of the variational deformation. We express the deformation mapping  $f_{\mathbf{a},\mathbf{b}}(\eta)$  in matrix form as:

$$f_{\mathbf{a},\mathbf{b}}(\eta)_{1 \times d} = (\Phi_{1 \times n} \quad \Psi_{1 \times m}) \begin{pmatrix} \mathbf{a}_{n \times d} \\ \mathbf{b}_{m \times d} \end{pmatrix}, \quad (51)$$

where  $d = 2, 3$ . Here,  $n = |I_V|$  denotes the number of vertices, and  $m = |I_T|$  represents the number of faces. The vector  $\Phi$  is a row vector composed of all Dirichlet terms  $\phi_v^{\mathbf{A}}(\eta)$ , and  $\Psi$  is a row vector composed of all Neumann terms  $\psi_t^{\mathbf{A}}(\eta)$ .

The Jacobian matrix  $\mathbf{J}_f(\eta)$  and the Hessian  $\mathbf{H}_f(\eta)$  of the deformation mapping  $f_{\mathbf{a},\mathbf{b}}(\eta)$  are also linear in  $\mathbf{a}$  and  $\mathbf{b}$ , and are expressed as follows:

$$(\mathbf{J}_f(\eta))_{d \times d} = ((\mathbf{G}_{\Phi})_{d \times n} \quad (\mathbf{G}_{\Psi})_{d \times m}) \begin{pmatrix} \mathbf{a}_{n \times d} \\ \mathbf{b}_{m \times d} \end{pmatrix}, \quad (52)$$

where each column of  $\mathbf{G}_{\Phi}$  captures the gradients of  $\phi_v^{\mathbf{A}}(\eta)$  for one vertex  $v$ , and each column of  $\mathbf{G}_{\Psi}$  records the gradients of  $\psi_t^{\mathbf{A}}(\eta)$  for one face  $t$ .

$$(\mathbf{H}_f(\eta))_{[d(d+1)/2] \times d} = \left( (\mathbf{H}_{\Phi})_{[d(d+1)/2] \times n} \quad (\mathbf{H}_{\Psi})_{[d(d+1)/2] \times m} \right) \begin{pmatrix} \mathbf{a}_{n \times d} \\ \mathbf{b}_{m \times d} \end{pmatrix}, \quad (53)$$

where each column of  $\mathbf{H}_{\Phi}$  records the elements of the Hessian matrix of  $\phi_v^{\mathbf{A}}(\eta)$ , comprising  $d(d+1)/2$  values. This vector is derived by flattening the symmetric Hessian matrix, retaining the diagonal elements and the upper-right components. Similarly,  $\mathbf{H}_{\Psi}$  contains the elements of the Hessian matrix of  $\psi_t^{\mathbf{A}}(\eta)$ . Since the solution to the anisotropic Laplacian equation also satisfies the boundary maximum principle, points for computing Hessians can be selected near the boundary, similar to previous methods

Based on the above formulation, we can now define an optimization framework. The energy functional  $E(f_{a,b})$  is designed to be as rigid as possible (ASAP) at specific points (typically medial axis points), to ensure global smoothness (by minimizing the Hessian magnitude), and to satisfy user constraints at certain points (i.e., deforming specific points to the positions defined by the user). For discrete sampling, this problem is formulated as:

$$\begin{aligned} \min_{\mathbf{a}, \mathbf{b}, \mathbf{R}_i} E(f_{a,b}) &= \sum_{i=1}^d \|\mathbf{J}_f(m_i) - \mathbf{R}_i\|_F^2 + \lambda_1 \sum_{i=1}^r \|f_{a,b}(q_i) - f_i\|_2^2 \\ &+ \lambda_2 \sum_{i=1}^k \|\mathbf{H}_f(w_i)\|_F^2 + \lambda_3 (\|\mathbf{a} - \mathbf{a}_0\|_F^2 + \|\mathbf{b} - \mathbf{b}_0\|_F^2), \quad (54) \\ \text{s.t. } \mathbf{R}_i^\top \mathbf{R}_i &= \mathbf{I}, \forall i = 1, \dots, d. \end{aligned}$$

Here,  $\mathbf{a}_0$  and  $\mathbf{b}_0$  represent the values of the source cage. The formulation here aligns more closely with Michel et al. [2025] than with the earlier work [Ben-Chen et al. 2009], which employs soft positional constraints  $\|f_{a,b}(q_i) - f_i\|_2^2$ ; however, experiments also demonstrate that soft constraints effectively satisfy the requirements. We also introduce a regularization term  $\|\mathbf{a} - \mathbf{a}_0\|_F^2 + \|\mathbf{b} - \mathbf{b}_0\|_F^2$  with a small value of  $\lambda_3$  to ensure minimal deviation while improving optimization stability. We apply the local/global strategy to solve this problem [Ben-Chen et al. 2009; Liu et al. 2008; Sorkine and Alexa 2007]. Specifically, in the local step, we fix  $\mathbf{a}$ ,  $\mathbf{b}$  and solve for the optimal rotation matrices  $\mathbf{R}_i$ . This is a well-known orthogonal Procrustes problem, which can be efficiently solved using singular value decomposition. In the global step, we fix  $\mathbf{R}_i$  and solve for  $\mathbf{a}$ ,  $\mathbf{b}$ . This constitutes an unconstrained least-squares problem, which can be straightforwardly transformed into a linear system.

The variational shape deformation presented in this section underscores the value of establishing the anisotropic Green coordinates formulation, especially when compared to the similarity Green deformation discussed in Section 5. We denote the deformation map of isotropic Green coordinates as  $f'_{a',b'}(\eta')$ . Based on the preceding analysis, the deformation mapping can be expressed as

$$f_{a,b}(\eta) = \mathbf{A}^{1/2} f'_{a',b'}(\mathbf{A}^{-1/2} \eta). \quad (55)$$

The gradient of  $f_{a,b}(\eta)$  can be expressed as

$$\nabla f_{a,b}(\eta) = \mathbf{A}^{1/2} \nabla f'(\mathbf{A}^{-1/2} \eta) \mathbf{A}^{-1/2}. \quad (56)$$

Then, if  $\mathbf{R}$  is a rotation matrix, the constraints  $\nabla f_{a,b}(\eta) = \mathbf{R}$  can be expressed as  $\nabla f'(\mathbf{A}^{-1/2} \eta) = \mathbf{A}^{-1/2} \mathbf{R} \mathbf{A}^{1/2}$ . However, the right-hand side is not necessarily a rotation matrix, since

$$(\mathbf{A}^{-1/2} \mathbf{R} \mathbf{A}^{1/2})^\top (\mathbf{A}^{-1/2} \mathbf{R} \mathbf{A}^{1/2}) = \mathbf{A}^{1/2} \mathbf{R}^\top \mathbf{A}^{-1} \mathbf{R} \mathbf{A}^{1/2}. \quad (57)$$

which does not necessarily equal  $\mathbf{I}$ . Consequently, it is challenging to formulate the local/global problem for the similarity Green transformation.

## 7 Experiments

This section presents the experimental results of our proposed method. First, we focus on cage-based deformation and demonstrate the results obtained with different coefficient matrices  $\mathbf{A}$ . Subsequently, we showcase variational deformation outcomes under the same constraints using varying  $\mathbf{A}$ . All experiments are performed

on a laptop equipped with an Intel CPU running at 2.40 GHz and 16GB of RAM.

We begin by describing the construction of different matrices  $\mathbf{A}$  for our experiments. First, we focus on the 2D scenario. Given that every symmetric positive definite matrix  $\mathbf{A}$  can be decomposed into a diagonal matrix  $\Lambda$  and a rotation matrix  $\mathbf{P} = \begin{pmatrix} \cos \theta & -\sin \theta \\ \sin \theta & \cos \theta \end{pmatrix}$  such that  $\mathbf{A} = \mathbf{P} \Lambda \mathbf{P}^\top$ , it suffices to specify different diagonal matrices  $\Lambda$  and rotation angles  $\theta$ . Therefore, we can denote  $\mathbf{A} = \mathcal{A}(\theta, \lambda_1, \lambda_2)$ . Moreover, in our formulation, we may assume one of the diagonal entries of the matrix to be 1.0, since for any  $c \in \mathbb{R}^+$ ,  $\nabla \cdot (\mathbf{A} \nabla u) = 0$  is equivalent to  $\nabla \cdot (c \mathbf{A} \nabla u) = 0$ . Consequently, both equations lead to the same deformation mapping. Appendix C.1 of the supplementary material provides some anisotropic matrices used in 2D deformation experiments together with the  $\lambda_1, \lambda_2, \theta$  values.

The construction of 3D matrices follows a similar approach. The 3D diagonal matrix  $\Lambda$  is defined by three parameters  $\lambda_1, \lambda_2$  and  $\lambda_3$ . The 3D rotation matrix  $\mathbf{P}$  is parameterized by three Euler angles  $\alpha, \beta, \gamma$  and can be expressed as  $\mathbf{P} = \mathbf{R}_z(\alpha) \mathbf{R}_y(\beta) \mathbf{R}_x(\gamma)$ , where

$$\begin{aligned} \mathbf{R}_z(\alpha) &= \begin{pmatrix} \cos \alpha & -\sin \alpha & 0 \\ \sin \alpha & \cos \alpha & 0 \\ 0 & 0 & 1 \end{pmatrix}, \quad \mathbf{R}_y(\beta) = \begin{pmatrix} \cos \beta & 0 & -\sin \beta \\ 0 & 1 & 0 \\ \sin \beta & 0 & \cos \beta \end{pmatrix}, \\ \mathbf{R}_x(\gamma) &= \begin{pmatrix} 1 & 0 & 0 \\ 0 & \cos \gamma & -\sin \gamma \\ 0 & \sin \gamma & \cos \gamma \end{pmatrix}. \end{aligned} \quad (58)$$

We can denote  $\mathbf{A} = \mathcal{A}(\lambda_1, \lambda_2, \lambda_3, \alpha, \beta, \gamma)$  for the 3D scenario.

### 7.1 Cage-based Deformation

We first present the results of anisotropic Green coordinates for cage-based deformation using various symmetric positive definite matrices  $\mathbf{A}$ . When  $\mathbf{A} = \mathbf{I}$ , the results are consistent with the isotropic Green coordinates [Lipman et al. 2008]. It should be noted that the isotropic method has many desirable properties, such as angle preservation. Thus, one cannot expect that applying an arbitrary matrix  $\mathbf{A}$  to induce anisotropic deformation will necessarily yield universally better results than the isotropic formulation. Nevertheless, our method still holds considerable value. This section begins with several representative examples to demonstrate the effects generated by different matrices  $\mathbf{A}$ , highlighting the diversity of deformation styles and options offered by our method. Additionally, we demonstrate scenarios in which anisotropic deformation potentials yield superior results—whether through enhanced visual quality, tighter adherence to the deformed cage, or reduced isotropic or area distortion. These advantages become more obvious when the input exhibits a high aspect ratio, where appropriate coefficient matrices achieves better outcomes. The formula for computing the distortion can be found in Section C.2.

We first conduct experiments on 2D images composed of cubic and circular shapes. In Fig. 4, we present the deformation results of a grid-like image under isotropic Green coordinates and anisotropic Green coordinates with eigenvalues of 1.0 and 4.0. The rotation matrices correspond to angles of  $\pi/6$  and  $\pi/3$ ; detailed parameter settings can be found in the table of Appendix C.1. We observe that different rotation matrices lead to “stretching” effects along different

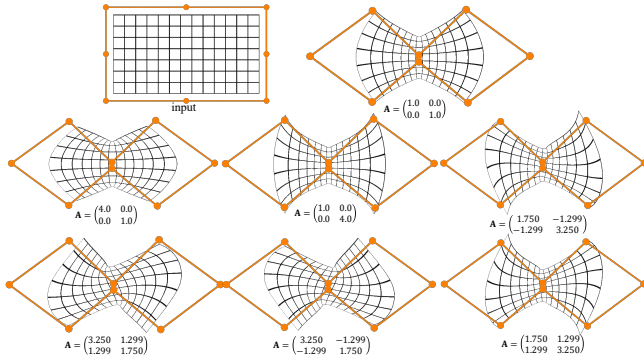


Fig. 4. Cage-based deformation of anisotropic Green coordinate in 2D. Different rotation matrices lead to “stretching” effects along different directions.

directions. Fig. 5 illustrates another example, in which the eigenvalues of the anisotropic coefficient matrix in the non-diagonal matrix are typically 1.0 and 2.0. The results demonstrate that isotropic Green coordinates are angle preserving and map infinitesimal circles to infinitesimal circles. However, the resulting effect are fixed, which also limits the flexibility and diversity of deformation. Our method enables a wide variety of deformation styles, and appropriate parameter settings can achieve desired effects. For instance, the leftmost image in the middle row of Fig. 5 minimizes area distortion.

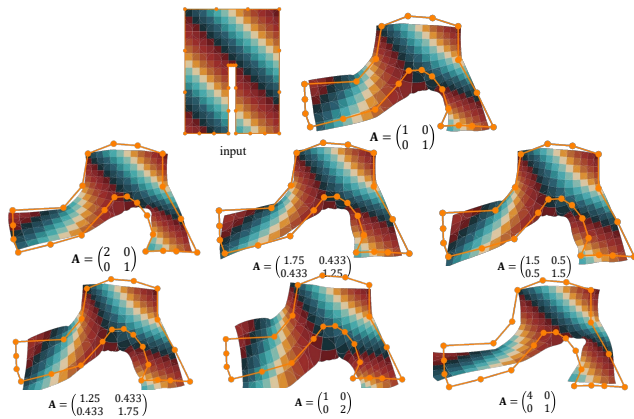


Fig. 5. Cage-based deformation results of an image containing circles and cubes.

Fig. 6, Fig. 7, and Fig. 8 show the cage-based deformation results of a fish, an elephant, and a giraffe model, respectively. It can be observed that different matrices control the “fatness” or “thinness” of the deformed objects and produce diverse deformation effects. The crab example in Fig. 9 further demonstrates that appropriate anisotropic settings can improve the deformation effect, exhibiting better consistency with the cage and resulting in more natural deformations compared to the input. Moreover, the anisotropic results exhibit lower isometric distortion (0.0245 vs. 0.0328) and area distortion (0.1340 vs. 0.1829).

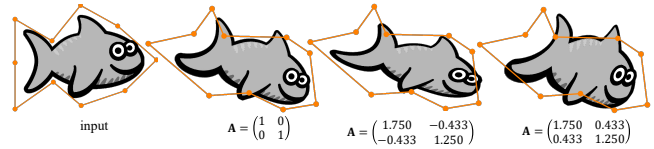


Fig. 6. Cage-based deformation results of a fish model.

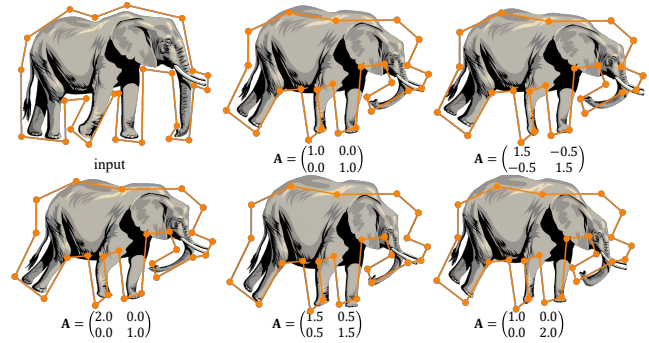


Fig. 7. Cage-based deformation results of an elephant model.

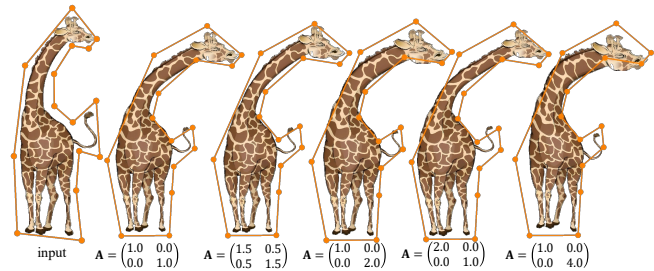


Fig. 8. Cage-based deformation results of a giraffe model.

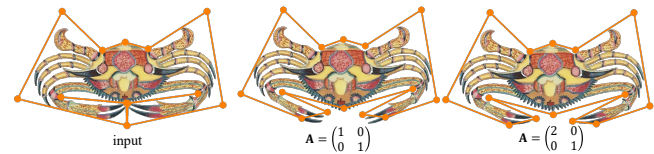


Fig. 9. Cage-based deformation results of a crab model.

Next, we move on to the results of 3D deformation. We first present the deformation of a bar model in Fig. 10, where the coordinate axes are indicated in the lower-left corner of the image. The deformation is mainly performed along the y-axis, while the long side is oriented along the z-axis. We show the anisotropic results aligned with both y-axis and z-axis. It can be observed that different matrices produce results with varying degrees of sharpness. Fig. 11 shows the results of a bench model, where different anisotropic matrices control the degree of “upward bending” in the chair’s cross-beam. In the skybox model of Fig. 12, the first row shows results for diagonal matrices, while the second row presents outcomes with

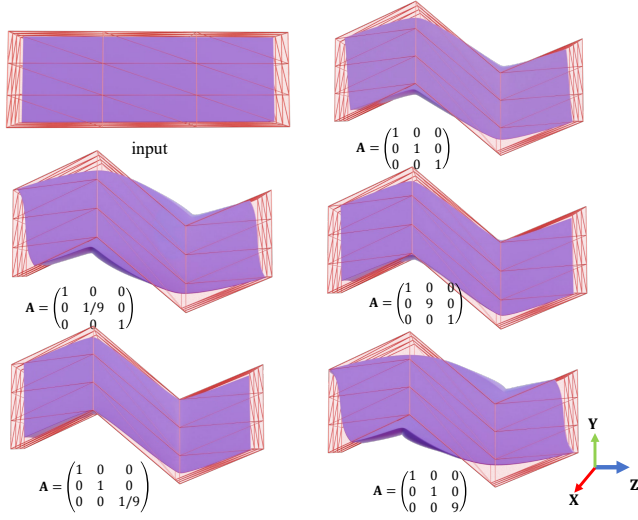


Fig. 10. Cage-based deformation results of a bar model in 3D.

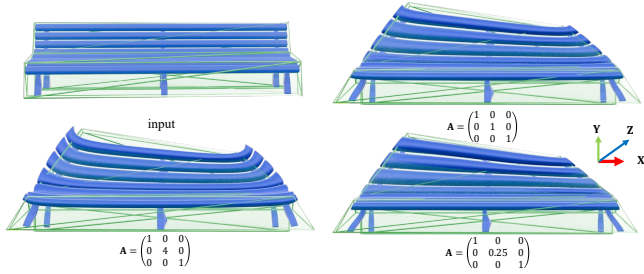


Fig. 11. Cage-based deformation results of a bench model in 3D.

non-diagonal matrices, specifically  $\mathbf{A} = \mathcal{A}(1.0, 0.25, 1.0, \pi/4, 0, 0)$ ,  $\mathbf{A} = \mathcal{A}(1.0, 0.25, 1.0, \pi/4, 0, \pi/4)$  and  $\mathbf{A} = \mathcal{A}(1.0, 0.25, 1.0, \frac{\pi}{3}, \frac{\pi}{4}, \frac{\pi}{6})$  from left to right. The experimental results further illustrate the wide range of deformation effects achieved by our approach.

## 7.2 Variational Shape Deformation

Here, we conduct experiments on variational shape deformation using different coefficient matrices. The method is reimplemented based on the technique proposed by [Ben-Chen et al. 2009] using Eq. (54). For the same input, all parameters are held constant except for the anisotropic matrix. Fig. 13 presents the results of variational shape deformation in 2D. The user-specified pre-deformation positions are indicated by red dots, while the target positions are marked with blue dots. The input cage is illustrated using orange-yellow lines. The parameters for the 2D deformation are configured as  $\lambda_1 = 100$ ,  $\lambda_2 = 10$  and  $\lambda_3 = 0.1$ . Additionally, 10 boundary points are sampled to compute the Hessian near each face for the first two inputs, while 2 are sampled near each face for the last input. The results show that varying the anisotropic matrices leads to different deformation outcomes, thereby broadening the range of deformation effects. Fig. 14 further shows the results of 3D variational deformation, where red and blue points are used to mark

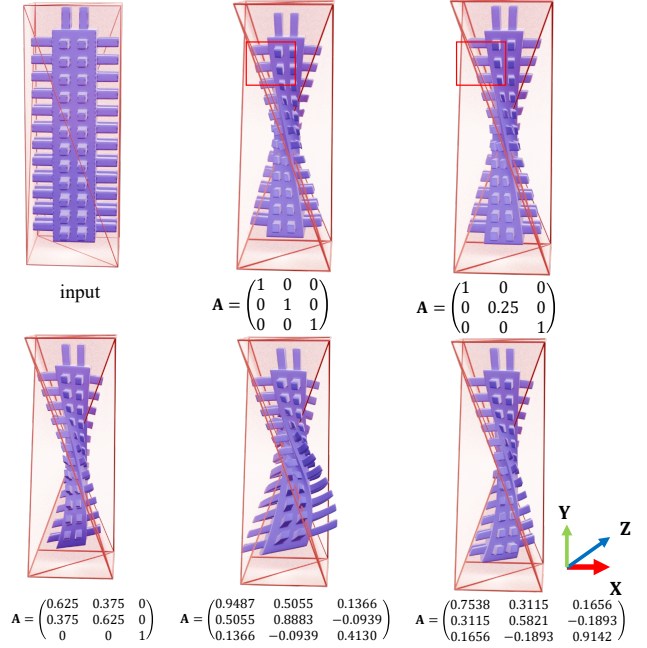


Fig. 12. Cage-based deformation results of a skybox model in 3D.

constraint points. We also manually annotate the constraint points that are occluded during rendering. For the Bar model, the parameters are set to  $\lambda_1 = 1000$ ,  $\lambda_2 = 0.5$  and  $\lambda_3 = 0.001$ , while for the Botijo model, the parameters are  $\lambda_1 = 100$ ,  $\lambda_2 = 0.05$  and  $\lambda_3 = 1.0$ . The results further illustrate the different effects produced by anisotropic deformations.

## 8 Conclusion

In this work, we introduce anisotropic Green coordinates, which incorporate a symmetric positive definite coefficient matrix within the divergence operator to enable diverse deformation styles in both cage-based deformation and variational shape deformation. We derive an integral identity formulation for the anisotropic Laplacian equation, ensuring that our method satisfies both linear reproduction and translation invariance. Moreover, anisotropic Green coordinates, along with their gradients and Hessians, admit closed-form expressions, enabling efficient deformation computation and supporting variational shape deformation with an as-rigid-as-possible energy term while accommodating user-specified positional constraints.

Our method still has certain limitations. The primary one is that  $\mathbf{A}$  remains globally invariant and has not been optimized for deformation constraints. Additionally, Green coordinates cannot simultaneously satisfy both Dirichlet and Neumann boundary conditions. We adopt Green coordinates as the foundation of our approach because of their theoretical elegance and strong compatibility with our concept of anisotropic deformation. It is our hope that this idea offers novel insights for anisotropic cage-based and variational deformation, and that this work inspires further research in the field.

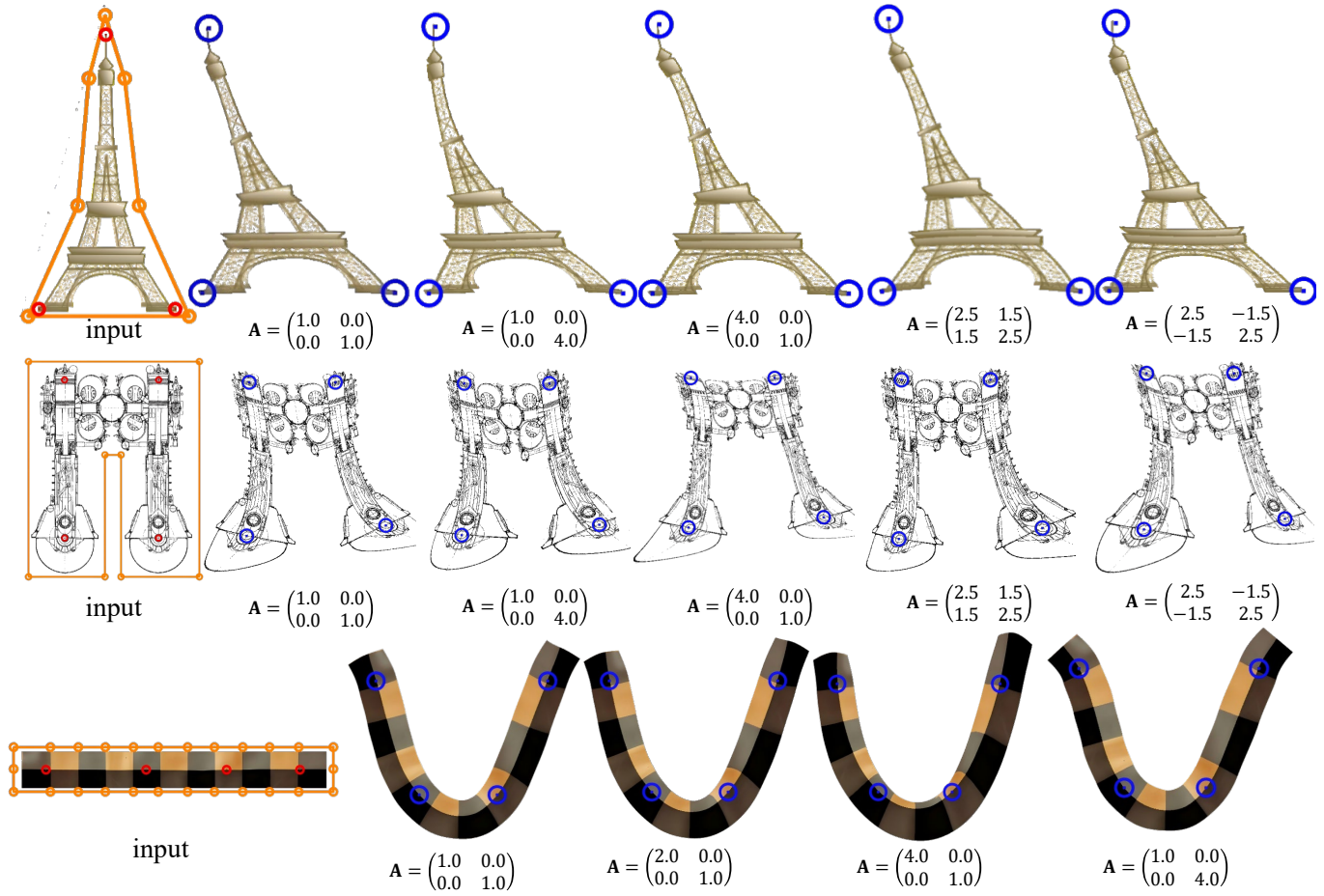


Fig. 13. Results of variational shape deformation in 2D. The red dots indicate the user-specified pre-deformation positions, while the blue dots mark the target positions.

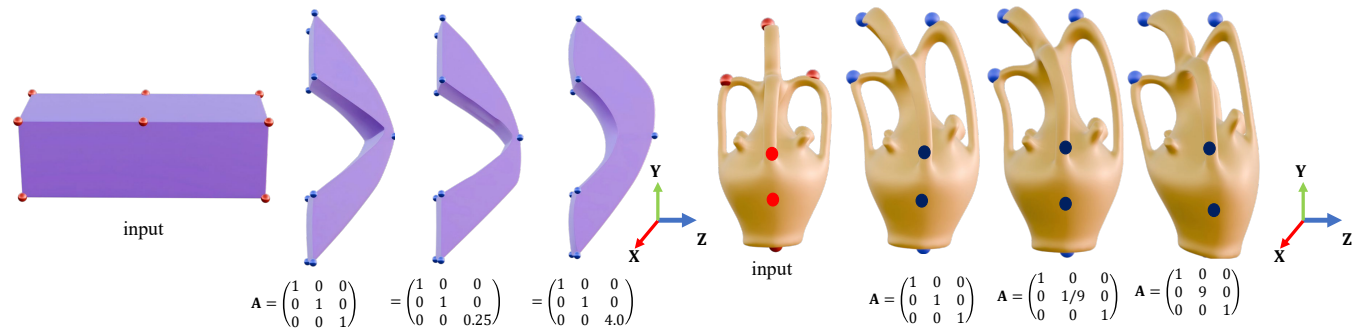


Fig. 14. Results of variational shape deformation in 3D.

## References

Alexander G. Belyaev. 2006. On transfinite barycentric coordinates. In *Proceedings of the Fourth Eurographics Symposium on Geometry Processing, Cagliari, Sardinia, Italy, June 26-28, 2006 (ACM International Conference Proceeding Series, Vol. 256)*, Alla Sheffer and Konrad Polthier (Eds.). Eurographics Association, 89–99.

Mirela Ben-Chen, Ofir Weber, and Craig Gotsman. 2009. Variational harmonic maps for space deformation. *ACM Transactions on Graphics* 28, 3 (2009), 34.

Qingjun Chang, Chongyang Deng, and Kai Hormann. 2023. Maximum likelihood coordinates. *Computer Graphics Forum* 42, 5 (2023), i–viii.

Qingjun Chang and Kai Hormann. 2025. Transfinite barycentric coordinates for arbitrary planar domains. *Comput. Aided Geom. Des.* 119 (2025), 102433.

- Jiong Chen and Mathieu Desbrun. 2022. Go Green: General Regularized Green's Functions for Elasticity. In *SIGGRAPH '22: Special Interest Group on Computer Graphics and Interactive Techniques Conference, Vancouver, BC, Canada, August 7 - 11, 2022*, Munkhtsetseg Nandigjav, Niloy J. Mitra, and Aaron Hertzmann (Eds.). ACM, 6:1–6:8.
- Tungyang Chen and Hsin-Yi Kuo. 2005. On linking  $n$ -dimensional anisotropic and isotropic Green's functions for infinite space, half-space, bimaterial, and multilayer for conduction. *International Journal of Solids and Structures* 42, 14 (2005), 4099–4114.
- Fernando de Goes and Mathieu Desbrun. 2024. Stochastic computation of barycentric coordinates. *ACM Transactions on Graphics* 43, 4 (2024), 42:1–42:13.
- Ana Dodik, Oded Stein, Vincent Sitzmann, and Justin Solomon. 2023. Variational barycentric coordinates. *ACM Transactions on Graphics* 42, 6 (2023), 255:1–255:16.
- Christopher Dyken and Michael S. Floater. 2009. Transfinite mean value interpolation. *Comput. Aided Geom. Des.* 26, 1 (2009), 117–134.
- Evans and C Lawrence. 1964. Partial differential equations. *Interscience Publishers* (1964).
- Michael S. Floater. 2003. Mean value coordinates. *Computer Aided Geometric Design* 20, 1 (2003), 19–27.
- Michael S. Floater. 2015. Generalized barycentric coordinates and applications. *Acta Numerica* 24 (2015), 161–214.
- Michael S. Floater, Géza Kós, and Martin Reimers. 2005. Mean value coordinates in 3D. *Computer Aided Geometric Design* 22, 7 (2005), 623–631.
- Gerald B. Folland. 1995. *Introduction to Partial Differential Equations* (2nd ed.). Princeton University Press.
- Kai Hormann and N. Sukumar. 2008. Maximum entropy coordinates for arbitrary polytopes. *Computer Graphics Forum* 27, 5 (2008), 1513–1520.
- Kai Hormann and Narayan Sukumar. 2017. *Generalized barycentric coordinates in computer graphics and computational mechanics* (1st ed.). CRC Press, Boca Raton, FL.
- Pushkar Joshi, Mark Meyer, Tony DeRose, Brian Green, and Tom Sanocki. 2007. Harmonic coordinates for character articulation. *ACM Transactions on Graphics* 26, 3 (2007), 71.
- Tao Ju, Scott Schaefer, and Joe D. Warren. 2005. Mean value coordinates for closed triangular meshes. *ACM Transactions on Graphics* 24, 3 (2005), 561–566.
- Liliya Kharevych, Patrick Mullen, Houman Owahdi, and Mathieu Desbrun. 2009. Numerical coarsening of inhomogeneous elastic materials. *ACM Trans. Graph.* 28, 3 (2009), 51.
- Theodore Kim, Fernando de Goes, and Hayley N. Iben. 2019. Anisotropic elasticity for inversion-safety and element rehabilitation. *ACM Trans. Graph.* 38, 4 (2019), 69:1–69:15.
- Xian-Ying Li and Shi-Min Hu. 2013. Poisson coordinates. *IEEE Transactions on Visualization and Computer Graphics* 19, 2 (2013), 344–352.
- Xian-Ying Li, Tao Ju, and Shi-Min Hu. 2013. Cubic mean value coordinates. *ACM Transactions on Graphics* 32, 4 (2013), 126:1–126:10.
- Huan Cheng Lin, Floyd M. Chitalu, and Taku Komura. 2024. Analytic rotation-invariant modelling of anisotropic finite elements. *ACM Trans. Graph.* 43, 5 (2024), 157:1–157:20.
- Zhehui Lin and Renjie Chen. 2024. Polynomial Cauchy coordinates for curved cages. In *SIGGRAPH Asia 2024 Conference Papers*. ACM, 67:1–67:8.
- Yaron Lipman and David Levin. 2009. Derivation and analysis of Green coordinates. *Computational Methods and Function Theory* 10, 1 (2009), 167.
- Yaron Lipman, David Levin, and Daniel Cohen-Or. 2008. Green coordinates. *ACM Transactions on Graphics* 27, 3 (2008), 78.
- Ligang Liu, Lei Zhang, Yin Xu, Craig Gotsman, and Steven J. Gortler. 2008. A Local/Global Approach to Mesh Parameterization. *Comput. Graph. Forum* 27, 5 (2008), 1495–1504.
- Shibo Liu, Tielin Dai, Ligang Liu, and Xiao-Ming Fu. 2025. Polynomial 2D Biharmonic Coordinates for High-order Cages. *ACM Trans. Graph.* 44, 4 (2025), 77:1–77:10.
- Shibo Liu, Ligang Liu, and Xiao-Ming Fu. 2024a. Polynomial 2D Green coordinates for high-order cages. *CoRR* abs/2408.06831 (2024). arXiv:2408.06831 <https://doi.org/10.48550/arXiv.2408.06831>
- Shibo Liu, Ligang Liu, and Xiao-Ming Fu. 2024b. Closed-form Cauchy Coordinates and Their Derivatives for 2D High-order Cages. *arXiv preprint* (2024). <https://arxiv.org/abs/2408.06831>
- Yueji Ma, Jialu Shen, Yanzun Meng, Dong Xiao, Zuoqiang Shi, and Bin Wang. 2025. Anisotropic Gauss Reconstruction and Global Orientation with Octree-based Acceleration. *Computer Graphics Forum* 44, 5 (2025), e70199.
- Élie Michel, Alec Jacobson, Siddhartha Chaudhuri, and Jean-Marc Thiery. 2025. Variational Green and Biharmonic Coordinates for 2D Polynomial Cages. *ACM Trans. Graph.* 44, 4 (2025), 76:1–76:20.
- Élie Michel and Jean-Marc Thiery. 2023. Polynomial 2D Green coordinates for polygonal cages. In *ACM SIGGRAPH 2023 Conference Proceedings*. ACM, 23:1–23:9.
- Houman Owahdi and Lei Zhang. 2007. Metric-based upscaling. *Communications on Pure and Applied Mathematics* 60, 5 (2007), 675–723.
- Ulrich Pinkall and Konrad Polthier. 1993. Computing Discrete Minimal Surfaces and Their Conjugates. *Exp. Math.* 2, 1 (1993), 15–36.
- Kaikai Qin, Yunhao Zhou, Chenhao Ying, Yajuan Li, and Chongyang Deng. 2024.  $C^0$  generalized Coons patches for high-order cage-based deformation. *ACM Transactions on Graphics* 43, 6 (2024).
- Yuxue Ren, Na Lei, Hang Si, and Xianfeng David Gu. 2018. A Construction of Anisotropic Meshes Based on Quasi-Conformal Mapping. In *27th International Meshing Roundtable, IMR 2018, Albuquerque, NM, USA, October 1-5, 2018 (Lecture Notes in Computational Science and Engineering, Vol. 127)*, Xevi Roca and Adrien Loseille (Eds.). Springer, 249–267.
- Olga Sorkine and Marc Alexa. 2007. As-rigid-as-possible surface modeling. In *Proceedings of the Fifth Eurographics Symposium on Geometry Processing, Barcelona, Spain, July 4-6, 2007 (ACM International Conference Proceeding Series, Vol. 257)*, Alexander G. Belyaev and Michael Garland (Eds.). Eurographics Association, 109–116.
- By Gilbert Strang. 2003. Introduction to Linear Algebra: Third Edition. *Introduction to Linear Algebra* 28, Supplement S1 (2003), S33–S47.
- Jean-Marc Thiery and Tamy Boubekeur. 2022. Green coordinates for triquad cages in 3D. In *SIGGRAPH Asia 2022 Conference Papers*. ACM, 38:1–38:8.
- Jean-Marc Thiery, Élie Michel, and Jiong Chen. 2024. Biharmonic coordinates and their derivatives for triangular 3D cages. *ACM Transactions on Graphics* 43, 4 (2024), 138:1–138:17.
- Masataka Urigo. 2000. Analytical Integrals of Fundamental Solution of Three-Dimensional Laplace Equation and Their Gradients. *Transactions of the Japan Society of Mechanical Engineers Series A* 66, 642 (2000), 254–260. in Japanese.
- Ofir Weber, Mirela Ben-Chen, and Craig Gotsman. 2009. Complex barycentric coordinates with applications to planar shape Deformation. *Computer Graphics Forum* 28, 2 (2009), 587–597.
- Ofir Weber, Roi Poranne, and Craig Gotsman. 2012. Biharmonic coordinates. *Computer Graphics Forum* 31, 8 (2012), 2409–2422.
- Xiongyu Wu, Shibo Liu, and Xiao-Ming Fu. 2025. Polynomial 3D Green coordinates and their derivatives for linear cages. *Computers & Graphics* 132 (2025), 104388.
- Dong Xiao and Renjie Chen. 2025. Flexible 3D Cage-based Deformation via Green Coordinates on Bézier Patches. *CoRR* abs/2501.14068 (2025). arXiv:2501.14068
- Zhipei Yan and Scott Schaefer. 2019. A family of barycentric coordinates for co-dimension 1 manifolds with simplicial facets. *Computer Graphics Forum* 38, 5 (2019), 75–83.
- Zichun Zhong, Xiaohu Guo, Wenping Wang, Bruno Lévy, Feng Sun, Yang Liu, and Weihua Mao. 2013. Particle-based anisotropic surface meshing. *ACM Trans. Graph.* 32, 4 (2013), 99:1–99:14.

## Supplementary Material of *Anisotropic Green Coordinates*

DONG XIAO, University of Science and Technology of China, China

RENJIE CHEN\*, University of Science and Technology of China, China

BAILIN DENG, Cardiff University, UK

### A Mathematical Details of Important Lemmas

In the main text, our derivation of the anisotropic Green coordinates relies on several lemmas. This section provides detailed derivations of these lemmas. Although many of these derivations are not mathematically advanced, they are non-trivial and may not be immediately obvious within the context of this research topic. Therefore, they are included here for clarity and completeness.

LEMMA A.1. *Let  $\mathbf{x}, \mathbf{y} \in \mathbb{R}^d$ , the matrix  $\mathbf{B} \in \mathbb{R}^{d \times d}$  is an invertible matrix such that  $\mathbf{y} = \mathbf{B}\mathbf{x}$ . Then, for a  $C^2$  scalar function  $f$  and a  $C^2$  vector-valued function  $\mathbf{F}$ , we have  $\nabla_{\mathbf{x}} f = \mathbf{B}^\top \nabla_{\mathbf{y}} f$ ,  $\mathbf{H}_{\mathbf{x}}(f) = \mathbf{B}^\top \mathbf{H}_{\mathbf{y}}(f) \mathbf{B}$  and  $\nabla_{\mathbf{x}} \cdot \mathbf{F} = \nabla_{\mathbf{y}} \cdot (\mathbf{B}\mathbf{F})$ . Here,  $\nabla_{\mathbf{x}} f$  and  $\mathbf{H}_{\mathbf{x}}(f)$  denote the gradient and Hessian of  $f$  with respect to  $\mathbf{x}$ , respectively, and  $\nabla_{\mathbf{x}} \cdot \mathbf{F}$  is the divergence of  $\mathbf{F}$  with respect to  $\mathbf{x}$ .*

PROOF. Since  $\mathbf{y} = \mathbf{B}\mathbf{x}$ , we have  $y_j = \sum_{k=1}^d B_{jk} x_k$  and  $\frac{\partial y_j}{\partial x_i} = B_{ji}$ . Therefore,

$$\frac{\partial f}{\partial x_i} = \sum_{j=1}^d \frac{\partial f}{\partial y_j} \frac{\partial y_j}{\partial x_i} = \sum_{j=1}^d \frac{\partial f}{\partial y_j} B_{ji}, \quad (1)$$

which is equivalent to  $\nabla_{\mathbf{x}} f = \mathbf{B}^\top \nabla_{\mathbf{y}} f$ .

Calculate the second derivative, we have

$$\frac{\partial^2 f}{\partial x_i \partial x_k} = \frac{\partial}{\partial x_i} \left( \sum_{j=1}^d \frac{\partial f}{\partial y_j} B_{jk} \right) = \sum_{j=1}^d B_{jk} \frac{\partial}{\partial x_i} \left( \frac{\partial f}{\partial y_j} \right) = \sum_{j=1}^d B_{jk} \sum_{l=1}^d \frac{\partial^2 f}{\partial y_j \partial y_l} \frac{\partial y_l}{\partial x_i} = \sum_{j,l=1}^d B_{jk} \frac{\partial^2 f}{\partial y_j \partial y_l} B_{li}. \quad (2)$$

This implies that  $(\mathbf{H}_{\mathbf{x}}(f)) = (\mathbf{B}^\top \mathbf{H}_{\mathbf{y}}(f) \mathbf{B})^\top = \mathbf{B}^\top \mathbf{H}_{\mathbf{y}}(f) \mathbf{B}$ , where the symmetry of  $\mathbf{H}_{\mathbf{y}}(f)$  ensures the equality.

Moreover, let  $\mathbf{F} = (F_1, \dots, F_d)^\top$ , we have

$$\nabla_{\mathbf{x}} \cdot \mathbf{F} = \sum_{i=1}^d \frac{\partial F_i}{\partial x_i} = \sum_{i=1}^d \sum_{j=1}^d \frac{\partial F_i}{\partial y_j} \frac{\partial y_j}{\partial x_i} = \sum_{i=1}^d \sum_{j=1}^d \frac{\partial F_i}{\partial y_j} B_{ji} = \sum_{j=1}^d \frac{\partial}{\partial y_j} \left( \sum_{i=1}^d B_{ji} F_i \right) = \nabla_{\mathbf{y}} \cdot (\mathbf{B}\mathbf{F}). \quad (3)$$

□

LEMMA A.2. *Let  $\mathbf{x} \in \mathbb{R}^d$ ,  $\mathbf{B} \in \mathbb{R}^{d \times d}$  be an invertible matrix and  $\delta(\mathbf{x})$  be the Dirac delta distribution satisfying  $\delta(\mathbf{x}) = 0$  for  $\mathbf{x} \neq \mathbf{0}$  and  $\int_{\mathbb{R}^d} \delta(\mathbf{x}) = 1$ . Then,*

$$\delta(\mathbf{B}\mathbf{x}) = \frac{1}{|\det \mathbf{B}|} \delta(\mathbf{x}). \quad (4)$$

PROOF. Let  $\mathbf{y} = \mathbf{B}\mathbf{x}$ , we have  $d\mathbf{y} = |\det \mathbf{B}| d\mathbf{x}$ . Moreover, let  $\varphi$  be an arbitrary smooth test function with compact support. Then,

$$\int_{\mathbb{R}^d} \delta(\mathbf{B}\mathbf{x}) \varphi(\mathbf{x}) d\mathbf{x} = \int_{\mathbb{R}^d} \delta(\mathbf{y}) \varphi(\mathbf{B}^{-1}\mathbf{y}) \frac{1}{|\det \mathbf{B}|} d\mathbf{y} = \frac{1}{|\det \mathbf{B}|} \varphi(\mathbf{0}) = \frac{1}{|\det \mathbf{B}|} \int_{\mathbb{R}^d} \delta(\mathbf{x}) \varphi(\mathbf{x}) d\mathbf{x}. \quad (5)$$

\*Corresponding author

Therefore, for all test functions  $\varphi$ :

$$\int_{\mathbb{R}^d} \delta(\mathbf{B}\mathbf{x})\varphi(\mathbf{x}) \, d\mathbf{x} = \frac{1}{|\det \mathbf{B}|} \int_{\mathbb{R}^d} \delta(\mathbf{x})\varphi(\mathbf{x}) \, d\mathbf{x}. \quad (6)$$

This implies that  $\delta(\mathbf{B}\mathbf{x}) = \frac{1}{|\det \mathbf{B}|} \delta(\mathbf{x})$ .  $\square$

LEMMA A.3. Let  $\mathbf{B}$  be an invertible matrix, and  $\mathbf{n}$  denote the normal vector of a 1-simplex in  $\mathbb{R}^2$  or 2-simplex in  $\mathbb{R}^3$ , denoted by  $C$ . If  $C$  is transformed by  $\mathbf{B}$ , i.e., all vertices  $\mathbf{v}_i$  of  $C$  are mapped to  $\mathbf{B}\mathbf{v}_i$ . Then, the normal vector of the transformed simplex  $C'$  is given by  $\frac{\mathbf{B}^{-\top}\mathbf{n}}{\|\mathbf{B}^{-\top}\mathbf{n}\|}$ .

PROOF. Let  $\mathbf{v}_1, \mathbf{v}_2 \in \mathbb{R}^2$ . By definition,  $\mathbf{n} \cdot (\mathbf{v}_2 - \mathbf{v}_1) = 0$ . Then,

$$(\mathbf{B}^{-\top}\mathbf{n}) \cdot (\mathbf{B}\mathbf{v}_2 - \mathbf{B}\mathbf{v}_1) = \mathbf{n}^{\top}\mathbf{B}^{-1}\mathbf{B}(\mathbf{v}_2 - \mathbf{v}_1) = \mathbf{n} \cdot (\mathbf{v}_2 - \mathbf{v}_1) = 0. \quad (7)$$

Therefore,  $\frac{\mathbf{B}^{-\top}\mathbf{n}}{\|\mathbf{B}^{-\top}\mathbf{n}\|}$  is the normal vector of  $C'$ .

Let  $\mathbf{v}_1, \mathbf{v}_2, \mathbf{v}_3 \in \mathbb{R}^3$ . By definition,  $\mathbf{n} \cdot (\mathbf{v}_2 - \mathbf{v}_1) = 0$  and  $\mathbf{n} \cdot (\mathbf{v}_3 - \mathbf{v}_1) = 0$ . Similarly to the 2D case, we have  $(\mathbf{B}^{-\top}\mathbf{n}) \cdot (\mathbf{B}\mathbf{v}_2 - \mathbf{B}\mathbf{v}_1) = 0$  and  $(\mathbf{B}^{-\top}\mathbf{n}) \cdot (\mathbf{B}\mathbf{v}_3 - \mathbf{B}\mathbf{v}_1) = 0$ . Therefore,  $\frac{\mathbf{B}^{-\top}\mathbf{n}}{\|\mathbf{B}^{-\top}\mathbf{n}\|}$  is the normal vector of  $C'$ .  $\square$

LEMMA A.4. Let  $C$  be a curve in  $\mathbb{R}^2$  parameterized by  $\mathbf{r}(u)$  with the length element  $ds = \|\mathbf{r}_u\| \, du$ .  $C'$  is the curve obtained by applying an invertible linear transformation  $\mathbf{B}$  to  $C$ , i.e.,  $C'$  is parameterized by  $\mathbf{s}(u) = \mathbf{B}\mathbf{r}(u)$ . Then the length element  $ds'$  of  $C'$  is given by:

$$ds' = \|\mathbf{B}\mathbf{t}(u)\| \, ds, \quad (8)$$

where  $\mathbf{t}(u)$  is the unit tangent vector to  $C$  at  $\mathbf{r}(u)$ . In particular, if  $\mathbf{B}$  is symmetric, we also have

$$ds' = |\det \mathbf{B}| \|\mathbf{B}^{-1}\mathbf{n}(u)\| \, ds, \quad (9)$$

where  $\mathbf{n}$  is the unit normal vector to  $C$  at  $\mathbf{r}(u)$ .

PROOF. The tangent vector of  $C'$  is  $\mathbf{s}_u = \mathbf{B}\mathbf{r}_u$ . The length element

$$ds' = \|\mathbf{s}_u\| \, du = \|\mathbf{B}\mathbf{r}_u\| \, du = \|\mathbf{B}\mathbf{t}(u)\| \|\mathbf{r}_u\| \, du = \|\mathbf{B}\mathbf{t}(u)\| \, ds. \quad (10)$$

where  $\mathbf{t}(u)$  is the unit tangent vector to  $C$  at  $\mathbf{r}(u)$ . This completes the proof of the first part.

Without loss of generality, we can choose an orthonormal coordinate system at  $\mathbf{r}(u)$  such that  $\mathbf{t}(u) = (1, 0)^{\top}$  and  $\mathbf{n}(u) = (0, 1)^{\top}$ . When  $\mathbf{B}$  is symmetric, it can be expressed as  $\mathbf{B} = \begin{pmatrix} a & b \\ b & c \end{pmatrix}$ . We also have  $\mathbf{B}^{-1} = \frac{1}{ac-b^2} \begin{pmatrix} c & -b \\ -b & a \end{pmatrix}$ .

Therefore,  $\|\mathbf{B}\mathbf{t}(u)\| = \sqrt{a^2 + b^2}$ . Given that  $|\det \mathbf{B}| = |ac - b^2|$ , we have

$$\|\mathbf{B}^{-1}\mathbf{n}(u)\| = \left\| \frac{1}{ac - b^2} (b, -a) \right\| = \frac{\sqrt{a^2 + b^2}}{|\det \mathbf{B}|} = \frac{\|\mathbf{B}\mathbf{t}(u)\|}{|\det \mathbf{B}|}. \quad (11)$$

This completes the proof of the second part.  $\square$

LEMMA A.5. Let  $C$  be a surface in  $\mathbb{R}^3$  parameterized by  $\mathbf{r}(u, v)$  with the area element  $ds = \|\mathbf{r}_u \times \mathbf{r}_v\| \, dudv$ .  $C'$  is the surface obtained by applying an invertible linear transformation  $\mathbf{B}$  to  $C$ , i.e.,  $C'$  is parameterized by  $\mathbf{s}(u, v) = \mathbf{B}\mathbf{r}(u, v)$ . Then the area element  $ds'$  of  $C'$  is given by:

$$ds' = |\det \mathbf{B}| \|\mathbf{B}^{-\top}\mathbf{n}(u, v)\| \, ds, \quad (12)$$

where  $\mathbf{n}(u, v)$  is the unit normal vector to  $C$  at  $\mathbf{r}(u, v)$ .

PROOF. The tangent vectors of  $C'$  are  $\mathbf{s}_u = \mathbf{B}\mathbf{r}_u$  and  $\mathbf{s}_v = \mathbf{B}\mathbf{r}_v$ . The area element on  $C'$  is given by  $ds' = \|\mathbf{s}_u \times \mathbf{s}_v\| dudv$ . We first show that

$$(\mathbf{B}\mathbf{a}) \times (\mathbf{B}\mathbf{b}) = (\det \mathbf{B})\mathbf{B}^{-\top}(\mathbf{a} \times \mathbf{b}) \quad (13)$$

for arbitrary vectors  $\mathbf{a}$  and  $\mathbf{b}$ . Consider another vector  $\mathbf{c} \in \mathbb{R}^3$  and the triple scalar product:

$$\begin{aligned} \mathbf{c} \cdot [(\mathbf{B}\mathbf{a}) \times (\mathbf{B}\mathbf{b})] &= \det(\mathbf{B}\mathbf{a}, \mathbf{B}\mathbf{b}, \mathbf{c}) = \det(\mathbf{B}) \det(\mathbf{a}, \mathbf{b}, \mathbf{B}^{-1}\mathbf{c}) \\ \det(\mathbf{B})(\mathbf{a} \times \mathbf{b}) \cdot (\mathbf{B}^{-1}\mathbf{c}) &= \det(\mathbf{B})(\mathbf{B}^{-\top}(\mathbf{a} \times \mathbf{b})) \cdot \mathbf{c}. \end{aligned} \quad (14)$$

Since  $\mathbf{c}$  is also arbitrary, we conclude that

$$(\mathbf{B}\mathbf{a}) \times (\mathbf{B}\mathbf{b}) = (\det \mathbf{B})\mathbf{B}^{-\top}(\mathbf{a} \times \mathbf{b}). \quad (15)$$

Therefore,

$$\mathbf{s}_u \times \mathbf{s}_v = (\mathbf{B}\mathbf{r}_u) \times (\mathbf{B}\mathbf{r}_v) = (\det \mathbf{B})\mathbf{B}^{-\top}(\mathbf{r}_u \times \mathbf{r}_v). \quad (16)$$

Taking the norms, we obtain

$$ds' = \|\mathbf{s}_u \times \mathbf{s}_v\| dudv = |\det \mathbf{B}| \|\mathbf{B}^{-\top}(\mathbf{r}_u \times \mathbf{r}_v)\| dudv = |\det \mathbf{B}| \|\mathbf{B}^{-\top} \mathbf{n}(u, v)\| \|\mathbf{r}_u \times \mathbf{r}_v\| dudv = |\det \mathbf{B}| \|\mathbf{B}^{-\top} \mathbf{n}(u, v)\| ds. \quad (17)$$

The third equality holds because  $\mathbf{n}(u, v) = \frac{\mathbf{r}_u \times \mathbf{r}_v}{\|\mathbf{r}_u \times \mathbf{r}_v\|}$ . This completes the proof.  $\square$

LEMMA A.6. *Let  $v_0, v_1, \dots, v_k$  be affinely independent points in  $\mathbb{R}^d$  with  $d \geq k$ , forming a  $k$ -simplex  $C$ . Then, the barycentric coordinates of any point  $p$  in  $C$  are unique with respect to  $v_0, v_1, \dots, v_k$ .*

PROOF. Suppose there exist two sets of barycentric coordinates  $(\lambda_0, \lambda_1, \dots, \lambda_k)$  and  $(\mu_0, \mu_1, \dots, \mu_k)$  such that:

$$p = \sum_{i=0}^k \lambda_i v_i = \sum_{i=0}^k \mu_i v_i, \quad (18)$$

where  $\lambda_i, \mu_i \geq 0$  and  $\sum_{i=0}^k \lambda_i = \sum_{i=0}^k \mu_i = 1$ . Subtracting the two representations gives

$$\sum_{i=0}^k (\lambda_i - \mu_i) v_i = 0. \quad (19)$$

Define  $\delta_i = \lambda_i - \mu_i$ . Then

$$\sum_{i=0}^k \delta_i v_i = 0 \quad \text{and} \quad \sum_{i=0}^k \delta_i = 0. \quad (20)$$

Reformulating using  $v_0$  as a reference point, we have

$$\sum_{i=0}^k \delta_i v_i = \sum_{i=0}^k \delta_i (v_i - v_0) + v_0 \sum_{i=0}^k \delta_i. \quad (21)$$

Since  $\sum_{i=0}^k \delta_i = 0$ , this simplifies to  $\sum_{i=1}^k \delta_i (v_i - v_0) = 0$ . By affine independence of the vertices, the vectors  $v_1 - v_0, \dots, v_k - v_0$  are linearly independent. Hence,  $\delta_i = 0$  for all  $i = 1, \dots, k$ . From  $\sum_{i=0}^k \delta_i = 0$ , it follows that  $\delta_0 = 0$  as well. Thus,  $\lambda_i = \mu_i$  for all  $i = 0, 1, \dots, k$ .  $\square$

## B Closed-Form Expressions of Isotropic Green Coordinates and Their Derivatives

In this section, we present detailed derivations of closed-form expressions for isotropic Green coordinates, including their gradients and Hessians, for both 2D and 3D oriented simplicial cages. These results form the foundation for the

development of anisotropic techniques. Although these results have appeared fragmentarily in previous literature [Ben-Chen et al. 2009; Lipman and Levin 2009; Lipman et al. 2008; Michel et al. 2025; Urago 2000], a systematic derivation and summary is still lacking. In particular, many publications in this field do not provide thorough derivations for the gradient and Hessian in the 3D scenario (Sec. B.2).

Mathematically, we denote the cage (2D or 3D) as  $P = (\mathbb{V}, \mathbb{T})$ , where  $\mathbb{V}$  denote the collection of the vertices and  $\mathbb{T}$  represent the collections of the face normals. Isotropic Green coordinates reproduce arbitrary point  $\eta$  within the cage using the cage vertices  $\{\mathbf{v}_i | i \in I_V\}$  and face normals  $\{\mathbf{n}(t_j) | j \in I_T\}$  as follows:

$$\eta = F(\eta, P) = \sum_{i \in I_V} \phi_i(\eta) \mathbf{v}_i + \sum_{j \in I_T} \psi_j(\eta) \mathbf{n}(t_j), \quad \eta \in \Omega, \quad (22)$$

where

$$\phi_i(\eta) = \int_{\xi \in \mathcal{N}\{\mathbf{v}_i\}} \Gamma_i(\xi) \frac{\partial G(\xi, \eta)}{\partial \mathbf{n}(\xi)} d\sigma_\xi, \quad i \in I_V, \quad (23)$$

$$\psi_j(\eta) = - \int_{\xi \in t_j} G(\xi, \eta) d\sigma_\xi, \quad j \in I_T. \quad (24)$$

Here,  $G(\xi, \eta)$  is the fundamental solution of the Laplacian equation, and  $\Gamma_i(\xi)$  is the hat-function, which equals one at vertex  $\mathbf{v}_i$ , zero at other vertices, and varies linearly over the one-ring neighborhood of  $\mathbf{v}_i$ . Our goal is to derive closed-form expressions for  $\phi_i(\eta)$ ,  $\psi_j(\eta)$ , as well as their gradients  $\nabla_\eta \phi_i(\eta)$ ,  $\nabla_\eta \psi_j(\eta)$ , and their Hessians  $H_\eta \phi_i(\eta)$ ,  $H_\eta \psi_j(\eta)$ . For brevity and clarity, we will omit the explicit dependence on  $\eta$  in the gradient and Hessian notations when no ambiguity arises.

### B.1 Isotropic Green coordinates for 2D

We begin by deriving the formulation for 2D, which mainly use the methods established in [Lipman and Levin 2009] and [Michel et al. 2025]. Fig. 1 provides an illustration of a 2D cage  $P$  along with its mathematical notations. We denote

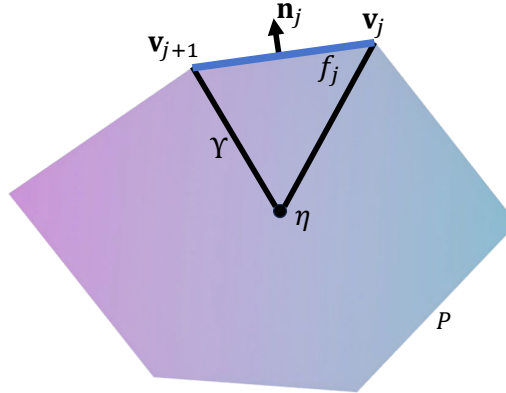


Fig. 1. The illustration of a 2D cage and its mathematical notations.

$f_j = \overrightarrow{\mathbf{v}_j \mathbf{v}_{j+1}}$  as one face of the cage. We first focus on computing  $\psi_j(\eta)$ , which is defined as the integral of  $-G(\xi, \eta)$  over

$f_j$ . We define  $\mathbf{a}_j = \mathbf{v}_{j+1} - \mathbf{v}_j$  and  $\mathbf{b}_j = \mathbf{v}_j - \eta$ . Consider the parametric curve  $\gamma(t) = \mathbf{v}_j + t\mathbf{a}_j$ , where  $t \in [0, 1]$ , we have:

$$\begin{aligned}\psi_j(\eta) &= - \int_{t_j} G(\xi, \eta) d\sigma_\xi = - \frac{1}{2\pi} \|\mathbf{a}_j\| \int_{t=0}^1 \log \|\mathbf{b}_j + t\mathbf{a}_j\| dt \\ &= - \frac{\|\mathbf{a}_j\|}{4\pi} \int_{t=0}^1 \log(\|\mathbf{a}_j\|^2 t^2 + 2(\mathbf{a}_j \cdot \mathbf{b}_j)t + \|\mathbf{b}_j\|^2) dt \\ &= - \frac{\|\mathbf{a}_j\|}{4\pi} (Q(1) - Q(0)),\end{aligned}\tag{25}$$

where  $Q(t)$  is the antiderivative of  $\log(\|\mathbf{a}_j\|^2 t^2 + 2(\mathbf{a}_j \cdot \mathbf{b}_j)t + \|\mathbf{b}_j\|^2)$ , which has the following expression [Lipman and Levin 2009]:

$$\begin{aligned}Q(t) &= \left( t + \frac{\mathbf{a}_j \cdot \mathbf{b}_j}{\|\mathbf{a}_j\|^2} \right) \log(\|\mathbf{a}_j\|^2 t^2 + 2(\mathbf{a}_j \cdot \mathbf{b}_j)t + \|\mathbf{b}_j\|^2) \\ &\quad - \left( \frac{\|\mathbf{a}_j\|^2 + (\mathbf{a}_j \cdot \mathbf{b}_j)}{\|\mathbf{a}_j\|^2 \sqrt{\|\mathbf{a}_j\|^2 \|\mathbf{b}_j\|^2 - (\mathbf{a}_j \cdot \mathbf{b}_j)^2}} \right) \arctan \left( \frac{\|\mathbf{a}_j\|^2 t + (\mathbf{a}_j \cdot \mathbf{b}_j)}{\sqrt{\|\mathbf{a}_j\|^2 \|\mathbf{b}_j\|^2 - (\mathbf{a}_j \cdot \mathbf{b}_j)^2}} \right).\end{aligned}\tag{26}$$

We now focus on the Dirichlet term  $\phi_{\mathbf{v}_j}(\eta)$ , which is defined on cage vertices  $\mathbf{v}_j$ . We denote  $\phi_{\mathbf{v}_j, f_j}(\eta)$  as the contribution of face  $f_j$  to  $\phi_{\mathbf{v}_j}(\eta)$ . The value of  $\phi_{\mathbf{v}_j}(\eta)$  is obtained by summing the contributions from all faces incident to  $\mathbf{v}_j$ . Recall that the parametric equation of  $f_j$  is  $\gamma(t) = \mathbf{v}_j + t\mathbf{a}_j$ , where  $t \in [0, 1]$ . Therefore,

$$\begin{aligned}\phi_{\mathbf{v}_j, f_j}(\eta) &= \int_0^1 (1-t) \left( \frac{\mathbf{a}_j t + \mathbf{b}_j}{2\pi \|\mathbf{a}_j t + \mathbf{b}_j\|^2} \cdot \mathbf{n}_j \right) \|\mathbf{a}_j\| dt \\ &= \frac{\|\mathbf{a}_j\| (\mathbf{b}_j \cdot \mathbf{n}_j)}{2\pi} \int_0^1 \frac{(1-t) dt}{\|\mathbf{a}_j\|^2 t^2 + 2t(\mathbf{a}_j \cdot \mathbf{b}_j) + \|\mathbf{b}_j\|^2} \\ &= - \frac{\|\mathbf{a}_j\| (\mathbf{b}_j \cdot \mathbf{n}_j)}{2\pi} (W(1) - W(0)),\end{aligned}\tag{27}$$

where  $W(t)$  is the antiderivative of  $\frac{t-1}{\|\mathbf{a}_j\|^2 t^2 + 2t(\mathbf{a}_j \cdot \mathbf{b}_j) + \|\mathbf{b}_j\|^2}$ , which is given by

$$W(t) = \frac{1}{2\|\mathbf{a}_j\|^2} \log(\|\mathbf{a}_j\|^2 t^2 + 2t(\mathbf{a}_j \cdot \mathbf{b}_j) + \|\mathbf{b}_j\|^2) - \left( \frac{\|\mathbf{a}_j\|^2 + (\mathbf{a}_j \cdot \mathbf{b}_j)}{\|\mathbf{a}_j\|^2 \sqrt{\|\mathbf{a}_j\|^2 \|\mathbf{b}_j\|^2 - (\mathbf{a}_j \cdot \mathbf{b}_j)^2}} \right) \arctan \left( \frac{\|\mathbf{a}_j\|^2 t + (\mathbf{a}_j \cdot \mathbf{b}_j)}{\sqrt{\|\mathbf{a}_j\|^2 \|\mathbf{b}_j\|^2 - (\mathbf{a}_j \cdot \mathbf{b}_j)^2}} \right).\tag{28}$$

We now proceed to compute the derivatives of  $\phi_{\mathbf{v}_j}(\eta)$  and  $\psi_j(\eta)$ . The core idea involves expressing these values in terms of integrals of rational functions with even-powered denominators with respect to the parameter  $t$ . The expressions are then subjected to partial fraction decomposition, and the integrals are evaluated using recurrence relations. Detailed derivations are provided in [Michel et al. 2025]; only the key steps are summarized here. Recall  $\gamma(t) = \mathbf{v}_j + t\mathbf{a}_j$ . Moreover, we denote  $\gamma_\eta(t) = \gamma(t) - \eta$ , then we have

$$\nabla_\eta \phi_{\mathbf{v}_j, f_j}(\eta) = - \frac{\|\mathbf{a}_j\|}{2\pi} \int_{t=0}^1 (1-t) \left[ \frac{\mathbf{n}_j}{\|\gamma_\eta(t)\|^2} - 2 \frac{(\gamma_\eta(t) \cdot \mathbf{n}_j) \gamma_\eta(t)}{\|\gamma_\eta(t)\|^4} \right] dt,\tag{29}$$

$$H_\eta \phi_{\mathbf{v}_j, f_j}(\eta) = - \frac{\|\mathbf{a}_j\|}{2\pi} \int_{t=0}^1 (1-t) \left[ 2 \frac{\mathbf{n}_j \gamma_\eta(t)^\top + \gamma_\eta(t) \mathbf{n}_j^\top}{\|\gamma_\eta(t)\|^4} + 2 \frac{(\gamma_\eta(t) \cdot \mathbf{n}_j) \mathbf{I}}{\|\gamma_\eta(t)\|^4} - 8 \frac{(\gamma_\eta(t) \cdot \mathbf{n}_j) \gamma_\eta(t) \gamma_\eta(t)^\top}{\|\gamma_\eta(t)\|^6} \right] dt,\tag{30}$$

$$\nabla_\eta \psi_j(\eta) = \frac{\|\mathbf{a}_j\|}{2\pi} \int_{t=0}^1 \frac{\gamma_\eta(t)}{\|\gamma_\eta(t)\|^2} dt,\tag{31}$$

$$H_\eta \psi_j(\eta) = - \frac{\|\mathbf{a}_j\|}{2\pi} \int_{t=0}^1 \frac{\|\gamma_\eta(t)\|^2 \mathbf{I} - 2\gamma_\eta(t) \gamma_\eta(t)^\top}{\|\gamma_\eta(t)\|^4} dt.\tag{32}$$

Then, we can transform the above calculation as the integral  $F_{K,n}^c = \int_0^1 \frac{t^n dt}{P_Y(t)^K}$ , where  $P_Y(t) = \|\gamma(t) - \eta\|^2$  is a polynomial of degree 2. Then, we can decompose  $\frac{1}{P_Y(t)^K}$  into a sum of single-root rational terms. The remaining terms are all of the form  $G_{a,b}(\omega) = \int_0^1 t^a (t - \omega)^b dt$ , which can be computed using the following recursive formulation  $G_{a,b}(\omega)$ :

If  $b = -1$ , we have

$$G_{a,-1}(\omega) = \omega^a D(\omega) + U_a(\omega), \quad (33)$$

where:

$$D(\omega) = \log(1 - \omega) - \log(-\omega), \quad U_a(\omega) = \sum_{k=0}^{a-1} \frac{\omega^k}{a - k}. \quad (34)$$

If  $a = 0$ ,

$$G_{0,b}(\omega) = \frac{1}{b+1} [(1 - \omega)^{b+1} - (-\omega)^{b+1}]. \quad (35)$$

If  $a > 0$  and  $b \neq -1$ , the recurrence relation is given by:

$$G_{a,b}(\omega) = \frac{1}{b+1} [(1 - \omega)^{b+1} - a G_{a-1,b+1}(\omega)]. \quad (36)$$

## B.2 Isotropic Green coordinates for 3D

We now proceed to the derivation of isotropic Green coordinates and their derivatives in three dimensions. This part constitutes a central focus of this section, as existing works in the field [Ben-Chen et al. 2009], including foundational studies such as [Urago 2000] have primarily provided final results while offering relatively limited elaboration on the derivation process. Consider the tetrahedron depicted in Fig. 2, which is formed by a query point  $\eta$  and a triangle  $t_j = \Delta \mathbf{v}_{j_1} \mathbf{v}_{j_2} \mathbf{v}_{j_3}$  of the 3D cage, along with other mathematical notations for relevant variables. We compute the Neumann term  $\psi_j(\eta)$  associated with the face  $t_j$ , as well as the  $\phi_{\mathbf{v}_{j_1}, t_j}(\eta)$ , together with their gradients and Hessians. Here,  $\phi_{\mathbf{v}_{j_1}, t_j}(\eta)$  represents the contribution of the face  $t_j$  to  $\phi_{\mathbf{v}_{j_1}}(\eta)$ . In subsequent derivations, column vectors are used by default, whereas row vectors are explicitly denoted by a transpose symbol.

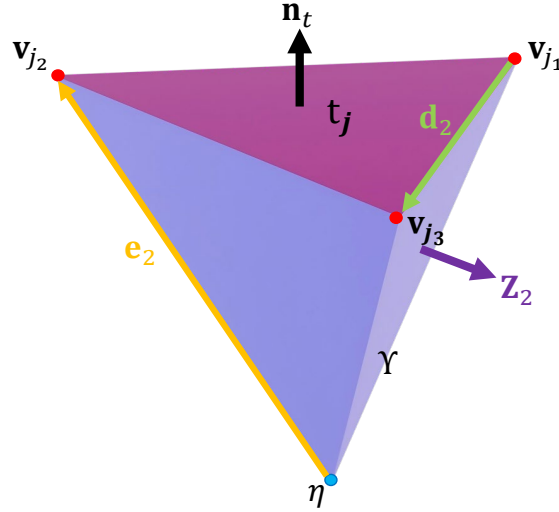


Fig. 2. A tetrahedron formed by a query point  $\eta$  and a triangle  $t_j = \Delta \mathbf{v}_{j_1} \mathbf{v}_{j_2} \mathbf{v}_{j_3}$  of the 3D cage, along with other mathematical notations for important variables.

To ensure clarity in subsequent expressions, we adopt the following notation. The tetrahedron formed by  $t$  and  $\eta$  is denoted as  $\Upsilon$ . The outward normal of  $t$  is denoted as  $\mathbf{n}_t$ . Additionally, we define  $\mathbf{e}_1 = \mathbf{v}_{j_1} - \eta$ ,  $\mathbf{e}_2 = \mathbf{v}_{j_2} - \eta$ ,  $\mathbf{e}_3 = \mathbf{v}_{j_3} - \eta$ , and their corresponding unit vectors as  $\bar{\mathbf{e}}_1 = \mathbf{e}_1/\|\mathbf{e}_1\|$ ,  $\bar{\mathbf{e}}_2 = \mathbf{e}_2/\|\mathbf{e}_2\|$  and  $\bar{\mathbf{e}}_3 = \mathbf{e}_3/\|\mathbf{e}_3\|$ . We also define  $R_1 = \|\mathbf{e}_2\| + \|\mathbf{e}_3\|$ ,  $R_2 = \|\mathbf{e}_3\| + \|\mathbf{e}_1\|$ ,  $R_3 = \|\mathbf{e}_1\| + \|\mathbf{e}_2\|$ ,  $\mathbf{d}_1 = \mathbf{v}_2 - \mathbf{v}_3$ ,  $\mathbf{d}_2 = \mathbf{v}_3 - \mathbf{v}_1$ ,  $\mathbf{d}_3 = \mathbf{v}_1 - \mathbf{v}_2$ ,  $\mathbf{Z}_1 = -\mathbf{e}_2 \times \mathbf{e}_3$ ,  $\mathbf{Z}_2 = -\mathbf{e}_3 \times \mathbf{e}_1$  and  $\mathbf{Z}_3 = -\mathbf{e}_1 \times \mathbf{e}_2$ . Additionally,  $\mathbf{z}_i = \mathbf{Z}_i/\|\mathbf{Z}_i\|$  denotes the unit outward normal vector of the side faces  $S_i$  for  $i = 1, 2, 3$ . In subsequent computations, the following quantities will also be frequently used:

$$C_i = \frac{1}{4\pi\|\mathbf{d}_i\|} \log\left(\frac{R_i + \|\mathbf{d}_i\|}{R_i - \|\mathbf{d}_i\|}\right), \quad \bar{C}_i = \frac{1}{2\pi(R_i + \|\mathbf{d}_i\|)(R_i - \|\mathbf{d}_i\|)}, \quad i = 1, 2, 3, \quad (37)$$

$$P_t = \mathbf{n}_t \times \sum_{i=1}^3 C_i \mathbf{d}_i - \omega_t \mathbf{n}_t, \quad (38)$$

where  $4\pi\omega_t$  is the signed solid angle of  $t_j$  toward  $\eta$ . We also define  $A_t$  as the area of  $t_j$ , and  $vol_t$  as the volume of the tetrahedron composed of  $t_j$  and  $\eta$ .  $H_t$  is the signed height of  $\eta$  to  $t_j$ . In our formulation, as shown in Fig. 2, when  $\eta$  is in the direction opposite to  $\mathbf{n}_j$ , we define  $\omega_t, H_t$  and  $vol_t$  as positive.

**1. Derivation of  $\psi_j(\eta)$ .** We first focus on the calculation of  $\psi_j(\eta)$ , which is the integral of  $-G(\xi, \eta)$  over  $t_j$  as

$$\psi_j(\eta) = - \int_{t_j} G(\xi, \eta) d\sigma_\xi, \quad (39)$$

we first begin with the divergence theorem of the tetrahedron  $\Upsilon$  as

$$\begin{aligned} \int_{\Upsilon} \nabla_\xi \cdot (G(\xi, \eta) \mathbf{n}_j) dV_\xi &= \int_{t_j+S_1+S_2+S_3} G(\xi, \eta) (\mathbf{n}_t \cdot \mathbf{n}(\xi)) d\sigma_\xi \\ &= \int_{t_j} G(\xi, \eta) d\sigma_\xi + (\mathbf{n}_t \cdot \mathbf{z}_1) \int_{S_1} G(\xi, \eta) d\sigma_\xi + (\mathbf{n}_t \cdot \mathbf{z}_2) \int_{S_2} G(\xi, \eta) d\sigma_\xi + (\mathbf{n}_t \cdot \mathbf{z}_3) \int_{S_3} G(\xi, \eta) d\sigma_\xi. \end{aligned} \quad (40)$$

The left-hand side of the above equation can be calculated as:

$$\begin{aligned} \int_{\Upsilon} \nabla_\xi \cdot (G(\xi, \eta) \mathbf{n}_t) dV_\xi &= \int_{\Upsilon} \nabla_\xi G(\xi, \eta) \cdot \mathbf{n}_t dV_\xi = \int_{h=0}^{H_t} \left( \int_{S(h)} \nabla_\xi G(\xi, \eta) \cdot \mathbf{n}_t dS \right) dh \\ &= \omega_t \int_{h=0}^{H_t} dh = \omega_t H_t = \frac{3\omega_t vol_t}{A_t}, \end{aligned} \quad (41)$$

Now we consider the integration of  $G(\xi, \eta)$  over the side face  $\triangle\eta\mathbf{v}_{j_1}\mathbf{v}_{j_2}$ , which is equivalent to the integration over  $\triangle\mathbf{O}\mathbf{v}'_{j_1}\mathbf{v}'_{j_2}$ , where  $\mathbf{O}$  is the origin,  $\mathbf{v}'_{j_1} = \mathbf{v}_{j_1} - \eta$  and  $\mathbf{v}'_{j_2} = \mathbf{v}_{j_2} - \eta$ . In Fig. 3, the region of integration is represented using polar coordinates  $R(\theta)$ . We also use  $\alpha, \beta$  and  $\theta$  to denote key angular variables in the figure. According to the law of sines, we have

$$R(\theta) = \frac{\|\mathbf{e}_1\| \sin(\alpha)}{\sin(\pi - \alpha - \theta)}. \quad (42)$$

Then, the integral of  $G(\xi, \eta)$  over  $\triangle\mathbf{O}\mathbf{v}'_{j_1}\mathbf{v}'_{j_2}$  can be computed as:

$$\begin{aligned} \int_{\triangle\mathbf{O}\mathbf{v}'_{j_1}\mathbf{v}'_{j_2}} G(\xi, \eta) d\sigma_\xi &= -\frac{1}{4\pi} \int_{\theta=0}^{\beta} \int_{r=0}^{R(\theta)} \frac{1}{r} \times r dr d\theta = -\frac{1}{4\pi} \int_{\theta=0}^{\beta} R(\theta) d\theta = -\frac{1}{4\pi} \int_{\theta=0}^{\beta} \frac{\|\mathbf{e}_1\| \sin(\alpha)}{\sin(\alpha + \theta)} d\theta. \\ &= -\frac{\|\mathbf{e}_1\| \sin(\alpha)}{4\pi} \int_{\theta=\alpha}^{\alpha+\beta} \csc \theta d\theta = -\frac{\|\mathbf{e}_1\| \sin(\alpha)}{8\pi} \log \left| \frac{1 - \cos \theta}{1 + \cos \theta} \right| \Bigg|_{\alpha}^{\alpha+\beta}. \end{aligned} \quad (43)$$

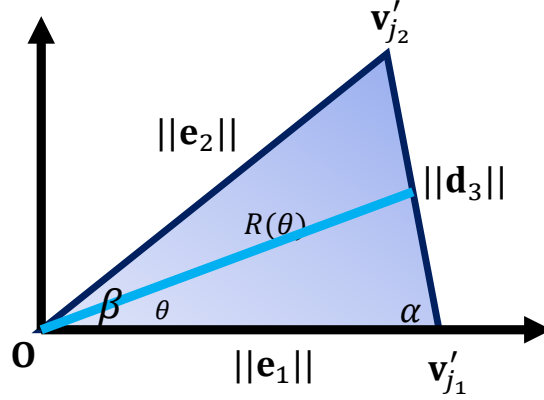


Fig. 3. Illustration of the integral of  $G(\xi, \eta)$  over the side face, along with other mathematical notations for important variables.

Additionally, we have

$$\cos(\alpha + \beta) = -\cos(\pi - \alpha - \beta) = \frac{\|\mathbf{e}_1\|^2 - \|\mathbf{e}_2\|^2 - \|\mathbf{d}_3\|^2}{2\|\mathbf{e}_2\|\|\mathbf{d}_3\|}, \quad \cos \alpha = \frac{\|\mathbf{d}_3\|^2 + \|\mathbf{e}_1\|^2 - \|\mathbf{e}_2\|^2}{2\|\mathbf{e}_1\|\|\mathbf{d}_3\|}. \quad (44)$$

Therefore,

$$\begin{aligned} \log \left| \frac{1 - \cos \theta}{1 + \cos \theta} \right| \Big|_{\alpha}^{\alpha + \beta} &= \log \frac{(\|\mathbf{e}_2\| + \|\mathbf{d}_3\|)^2 - \|\mathbf{e}_1\|^2}{\|\mathbf{e}_1\|^2 - (\|\mathbf{e}_2\| - \|\mathbf{d}_3\|)^2} - \log \frac{(\|\mathbf{e}_1\| + \|\mathbf{d}_3\|)^2 - \|\mathbf{e}_2\|^2}{\|\mathbf{e}_2\|^2 - (\|\mathbf{e}_1\| - \|\mathbf{d}_3\|)^2} \\ &= 2 \log \frac{\|\mathbf{e}_1\| + \|\mathbf{e}_2\| + \|\mathbf{d}_3\|}{\|\mathbf{e}_1\| + \|\mathbf{e}_2\| - \|\mathbf{d}_3\|}. \end{aligned} \quad (45)$$

Thus,

$$\int_{\Delta O\mathbf{v}'_{j_1}\mathbf{v}'_{j_2}} G(\xi, \eta) d\sigma_{\xi} = -\frac{\|\mathbf{e}_1\| \sin(\alpha)}{8\pi} \log \left| \frac{1 - \cos \theta}{1 + \cos \theta} \right| \Big|_{\alpha}^{\alpha + \beta} = -\frac{\|\mathbf{e}_1 \times \mathbf{e}_2\|}{4\pi\|\mathbf{d}_3\|} \log \frac{\|\mathbf{e}_2\| - \|\mathbf{e}_1\| + \|\mathbf{d}_3\|}{\|\mathbf{e}_1\| - \|\mathbf{e}_2\| + \|\mathbf{d}_3\|}. \quad (46)$$

The integral of  $G(\xi, \eta)$  over  $\Delta O\mathbf{v}'_{j_2}\mathbf{v}'_{j_3}$  and  $\Delta O\mathbf{v}'_{j_3}\mathbf{v}'_{j_1}$  can be evaluated using the same approach. Then, we can obtain the closed-form formula for  $\psi_j(\eta)$  as

$$\begin{aligned} \psi_j(\eta) &= - \int_{t_j} G(\xi, \eta) d\sigma_{\xi} = -\frac{1}{4\pi} \left( \frac{\mathbf{e}_1 \times \mathbf{e}_2}{\|\mathbf{d}_3\|} \log \frac{\|\mathbf{e}_1\| + \|\mathbf{e}_2\| + \|\mathbf{d}_3\|}{\|\mathbf{e}_1\| + \|\mathbf{e}_2\| - \|\mathbf{d}_3\|} \right. \\ &\quad \left. + \frac{\mathbf{e}_2 \times \mathbf{e}_3}{\|\mathbf{d}_1\|} \log \frac{\|\mathbf{e}_2\| + \|\mathbf{e}_3\| + \|\mathbf{d}_1\|}{\|\mathbf{e}_2\| + \|\mathbf{e}_3\| - \|\mathbf{d}_1\|} + \frac{\mathbf{e}_3 \times \mathbf{e}_1}{\|\mathbf{d}_2\|} \log \frac{\|\mathbf{e}_3\| + \|\mathbf{e}_1\| + \|\mathbf{d}_2\|}{\|\mathbf{e}_3\| + \|\mathbf{e}_1\| - \|\mathbf{d}_2\|} \right) \cdot \mathbf{n}_t - \frac{3}{A_t} \omega_t \text{vol}_t. \end{aligned} \quad (47)$$

Therefore,

$$\psi_t(\eta) = - \sum_{i=1}^3 C_i (\mathbf{Z}_i \cdot \mathbf{n}_t) - \frac{3}{A_t} \omega_t \text{vol}_t. \quad (48)$$

**2. Derivation of  $\phi_{\mathbf{v}_{j_1}, t_j}(\eta)$ .** Now, we focus on the derivation of  $\phi_{\mathbf{v}_{j_1}, t}(\eta)$ . We begin by extending the hat-function  $\Gamma_{\mathbf{v}_{j_1}, t_j}(\xi)$  from face  $t_j$  to the entire volume of  $\Upsilon$ . Recall that  $\Gamma_{\mathbf{v}_{j_1}, t_j}(\xi)$  takes the value 1 at  $\mathbf{v}_{j_1}$ , 0 at its adjacent vertices, and varies linearly within the 1-neighborhood of  $\mathbf{v}_{j_1}$ . Mathematically, for  $\xi \in \Upsilon$ ,  $\Gamma_{\mathbf{v}_{j_1}, t_j}(\xi)$  is given by 1.0 minus the ratio of the volumes of the tetrahedron  $\xi, \mathbf{v}_{j_2}, \mathbf{v}_{j_3}, \eta$  and  $\mathbf{v}_{j_1}, \mathbf{v}_{j_2}, \mathbf{v}_{j_3}, \eta$ . We also define  $\mathbf{q}$  as the foot of the perpendicular from  $\mathbf{v}_{j_1}$  to the plane spanned by  $\mathbf{v}_{j_2}, \mathbf{v}_{j_3}$  and  $\eta$ . Then,  $\Gamma_{\mathbf{v}_{j_1}, t_j}(\xi) = 1 - \frac{(\xi - \mathbf{v}_{j_1}) \cdot (\mathbf{q} - \mathbf{v}_{j_1})}{\|\mathbf{q} - \mathbf{v}_{j_1}\|^2}$ . Based on the relationships between the

cross product, scalar triple product, and their geometric interpretations in terms of area and volume, the gradient of  $\Gamma_{\mathbf{v}_{j_1, t_j}}(\xi)$  can be computed as

$$\nabla_{\xi} \Gamma_{\mathbf{v}_{j_1, t_j}}(\xi) = \frac{\mathbf{v}_{j_1} - \mathbf{q}}{\|\mathbf{v}_{j_1} - \mathbf{q}\|^2} = \frac{\mathbf{e}_2 \times \mathbf{e}_3}{\|\mathbf{e}_2 \times \mathbf{e}_3\|} \cdot \frac{\|\mathbf{e}_2 \times \mathbf{e}_3\|}{|\mathbf{e}_1 \cdot (\mathbf{e}_2 \times \mathbf{e}_3)|} = \frac{\mathbf{e}_2 \times \mathbf{e}_3}{|\mathbf{e}_1 \cdot (\mathbf{e}_2 \times \mathbf{e}_3)|} = -\frac{\mathbf{Z}_1}{6 \text{ vol}_t}. \quad (49)$$

According to the divergence theorem,

$$\int_{\partial Y} \Gamma_{\mathbf{v}_{j_1, t_j}}(\xi) \frac{\partial G}{\partial \mathbf{n}}(\xi) d\sigma_{\xi} = \int_Y \nabla_{\xi} \cdot (\Gamma_{\mathbf{v}_{j_1, t_j}}(\xi) \nabla_{\xi} G(\xi, \eta)) dV_{\xi}. \quad (50)$$

We denote  $\mathbf{z}_i = \mathbf{Z}_i / \|\mathbf{Z}_i\|$  the unit side normal vectors. We also observe that  $\nabla_{\xi} G(\xi, \eta) \cdot \mathbf{z}_j = 0$  in  $S_j$ ,  $j = 1, 2, 3$ . Therefore, computing  $\phi_{\mathbf{v}_{j_1, t}}(\eta)$  is equivalent to evaluating the right-hand side of Eq. (50). Moreover,

$$\nabla_{\xi} \cdot (\Gamma_{\mathbf{v}_{j_1, t_j}}(\xi) \nabla_{\xi} G(\xi, \eta)) = \Gamma_{\mathbf{v}_{j_1, t_j}}(\xi) \Delta_{\xi} G(\xi, \eta) + \nabla_{\xi} G(\xi, \eta) \cdot \nabla_{\xi} \Gamma_{\mathbf{v}_{j_1, t_j}}(\xi). \quad (51)$$

Since  $\nabla_{\xi} G(\xi, \eta) = \delta(\xi - \eta)$ , the integration of the first term in the equation above yields only  $\Gamma_{\mathbf{v}_{j_1, t_j}}(\eta)$ , which is vanish at  $\eta$ . Thus, we only need to compute

$$\int_Y \nabla_{\xi} G(\xi, \eta) \nabla_{\xi} \Gamma_{\mathbf{v}_{j_1, t_j}}(\xi) dV_{\xi} = -\frac{\mathbf{Z}_1}{6 \text{ vol}_t} \cdot \int_Y \nabla_{\xi} G(\xi, \eta) dV_{\xi}. \quad (52)$$

According to the component-wise application of the divergence theorem, we have

$$\int_Y \nabla_{\xi} G(\xi, \eta) dV_{\xi} = \int_{\partial Y} G(\xi, \eta) \mathbf{n}(\xi) d\sigma_{\xi} = \mathbf{n}_t \int_{t_j} G(\xi, \eta) d\sigma_{\xi} + \mathbf{z}_1 \int_{S_1} G(\xi, \eta) d\sigma_{\xi} + \mathbf{z}_2 \int_{S_2} G(\xi, \eta) d\sigma_{\xi} + \mathbf{z}_3 \int_{S_3} G(\xi, \eta) d\sigma_{\xi}. \quad (53)$$

According to previous calculation,  $\mathbf{z}_i \int_{S_i} G(\xi, \eta) d\sigma_{\xi} = -C_i \mathbf{Z}_i$ ,  $i = 1, 2, 3$ . If we denote  $\mathbf{L} = \int_Y \nabla G(\xi, \eta) dV_{\xi}$ , we have

$$\mathbf{L} = -\psi_t(\eta) \mathbf{n}_t - \sum_{i=1}^3 C_i \mathbf{Z}_i. \quad (54)$$

Taking the dot product with  $\mathbf{Z}_1$  gives

$$\begin{aligned} \mathbf{Z}_1 \cdot \mathbf{L} &= -\left( \sum_{i=1}^3 -C_i (\mathbf{Z}_i \cdot \mathbf{n}_t) - \frac{3}{A_t} \omega_t \text{vol}_t \right) (\mathbf{Z}_1 \cdot \mathbf{n}_t) - \sum_{i=1}^3 C_i (\mathbf{Z}_1 \cdot \mathbf{Z}_i) \\ &= -\sum_{i=1}^3 C_i \left( \mathbf{Z}_1 \cdot \mathbf{Z}_i - (\mathbf{Z}_1 \cdot \mathbf{n}_t) (\mathbf{Z}_i \cdot \mathbf{n}_t) \right) + \frac{3}{A_t} \omega_t \text{vol}_t (\mathbf{Z}_1 \cdot \mathbf{n}_t). \end{aligned} \quad (55)$$

We will now use the coordinate system method to prove the following important equation:

$$\mathbf{Z}_i - (\mathbf{Z}_i \cdot \mathbf{n}_t) \mathbf{n}_t = H_t (\mathbf{n}_t \times \mathbf{d}_i), \quad (56)$$

where  $H_t = \frac{3 \text{vol}_t}{A_t}$  is the height from  $\eta$  to  $t_j$ . We place  $t$  in the plane  $z = 0$  with outward unit normal  $\mathbf{n}_t = (0, 0, 1)$ . Then, we denote  $\mathbf{v}_{j_k} = (x_k, y_k, 0)$  for  $k = 1, 2, 3$ . We also locate  $\eta$  on  $z$ -axis and denote  $\eta = (0, 0, -H_t)$ . Then,  $\mathbf{e}_i = \mathbf{v}_{j_i} - \eta = (x_i, y_i, H_t)$ ,  $\mathbf{d}_i = \mathbf{v}_{j_{i+1}} - \mathbf{v}_{j_{i+2}} = (x_{i+1} - x_{i+2}, y_{i+1} - y_{i+2}, 0)$ . Note that indices greater than 3 should be taken modulo 3. Let  $a = x_{i+1} - x_{i+2}$ ,  $b = y_{i+1} - y_{i+2}$ , we have

$$\mathbf{Z}_i = -\mathbf{e}_{i+1} \times \mathbf{e}_{i+2} = -\mathbf{e}_{i+1} \times (\mathbf{e}_{i+1} - \mathbf{d}_i) = \mathbf{e}_{i+1} \times \mathbf{d}_i = (-H_t b, H_t a, x_{i+1} b - y_{i+1} a). \quad (57)$$

Therefore, we have  $\mathbf{Z}_i - (\mathbf{Z}_i \cdot \mathbf{n}_t) \mathbf{n}_t = (-H_t b, H_t a, 0)$ . On the other hand,

$$H_t (\mathbf{n}_t \times \mathbf{d}_i) = H_t \cdot ((0, 0, 1) \times (a, b, 0)) = (-H_t b, -H_t a, 0). \quad (58)$$

We complete the proof of the equation  $\mathbf{Z}_1 - (\mathbf{Z}_1 \cdot \mathbf{n}_t)\mathbf{n}_t = H_t(\mathbf{n}_t \times \mathbf{d}_i)$ . Then, we have

$$\begin{aligned}
\mathbf{Z}_1 \cdot \mathbf{L} &= - \sum_{i=1}^3 C_i \left( \mathbf{Z}_1 \cdot \mathbf{Z}_i - (\mathbf{Z}_1 \cdot \mathbf{n}_t)(\mathbf{Z}_i \cdot \mathbf{n}_t) \right) + \frac{3}{A_t} \omega_t \text{vol}_t(\mathbf{Z}_1 \cdot \mathbf{n}_t) \\
&= - \sum_{i=1}^3 C_i \left( \mathbf{Z}_1 \cdot (\mathbf{Z}_i - (\mathbf{Z}_i \cdot \mathbf{n}_t)\mathbf{n}_t) \right) + \frac{3}{A_t} \omega_t \text{vol}_t(\mathbf{Z}_1 \cdot \mathbf{n}_t) \\
&= - \sum_{i=1}^3 C_i \left( \mathbf{Z}_1 \cdot H_t(\mathbf{n}_t \times \mathbf{d}_i) \right) + \frac{3}{A_t} \omega_t \text{vol}_t(\mathbf{Z}_1 \cdot \mathbf{n}_t) \\
&= - \frac{3 \text{vol}_t}{A_t} \left( \mathbf{n}_t \times \sum_{i=1}^3 C_i \mathbf{d}_i - \omega_t \mathbf{n}_t \right) \cdot \mathbf{Z}_1.
\end{aligned} \tag{59}$$

Recall the definition  $P_t = \mathbf{n}_t \times \sum_{i=1}^3 C_i \mathbf{d}_i - \omega_t \mathbf{n}_t$ , we get

$$\phi_{\mathbf{v}_{j_1, t_j}}(\eta) = -\frac{1}{6 \text{vol}_t} \mathbf{Z}_1 \cdot \mathbf{L} = \frac{1}{2A_t} P_t \cdot \mathbf{Z}_1. \tag{60}$$

Therefore,

$$\boxed{\phi_{\mathbf{v}_{j_1, t_j}}(\eta) = \frac{1}{2A_t} P_t \cdot \mathbf{Z}_1.} \tag{61}$$

**3. Derivation of  $\nabla \psi_t(\eta)$ .** We now show that  $\mathbf{a} \cdot \nabla \psi_t(\eta) = -\mathbf{a} \cdot P_t$  for arbitrary vector  $\mathbf{a} \in \mathbb{R}^3$ . We first notice that  $\nabla_\eta G(\xi, \eta) = -\nabla_\xi G(\xi, \eta)$ . Therefore,

$$\mathbf{a} \cdot \nabla_\eta \psi_t(\eta) = -\mathbf{a} \cdot \int_{t_j} \nabla_\eta G(\xi, \eta) d\sigma_\xi = \int_{t_j} \mathbf{a} \cdot \nabla_\xi G(\xi, \eta) d\sigma_\xi. \tag{62}$$

The vector  $\mathbf{a}$  can be decomposed into tangential parts  $\mathbf{a}_\parallel$  and normal parts  $\mathbf{a}_\perp$  with respect to  $t_j$  as  $\mathbf{a}_\perp = (\mathbf{a} \cdot \mathbf{n}_t)\mathbf{n}_t$  and  $\mathbf{a}_\parallel = \mathbf{a} - \mathbf{a}_\perp$ . We define a tangential vector field  $\mathbf{F}(\xi)$  with respect to  $\xi$  at  $t_j$  as:

$$\mathbf{F}(\xi) = G(\xi, \eta) \mathbf{a}_\parallel. \tag{63}$$

Moreover, let  $\nabla_t \cdot$  be the planar divergence operator on  $t_j$ , we have  $\nabla_t \cdot \mathbf{F} = \nabla_t \cdot (G \mathbf{a}_\parallel) = \mathbf{a}_\parallel \cdot \nabla_t G$ . Since  $\nabla_t G$  is the tangential projection of  $\nabla_\xi G$ , we also have  $\mathbf{a}_\parallel \cdot \nabla_t G = \mathbf{a}_\parallel \cdot \nabla_\xi G$  on  $t_j$ . Therefore,

$$\int_{t_j} \mathbf{a}_\parallel \cdot \nabla_\xi G d\sigma = \int_{t_j} \nabla_t \cdot (G \mathbf{a}_\parallel) d\sigma = \int_{\partial t_j} G(\xi, \eta) (\mathbf{a}_\parallel \cdot \nu) ds, \tag{64}$$

where  $\nu$  is the outward unit co-normal along  $\partial t_j$  lying in the plane of  $t_j$ , and  $ds$  is the arc-length measure. Then,  $\nu_i = \mathbf{n}_t \times \frac{\mathbf{d}_i}{\|\mathbf{d}_i\|}$  for  $i = 1, 2, 3$ , and

$$\mathbf{a}_\parallel \cdot \nu_i = \mathbf{a} \cdot \left( \mathbf{n}_t \times \frac{\mathbf{d}_i}{\|\mathbf{d}_i\|} \right) = (\mathbf{a} \times \mathbf{n}_t) \cdot \frac{\mathbf{d}_i}{\|\mathbf{d}_i\|}. \tag{65}$$

Eq. (64) yields

$$\int_{t_j} \mathbf{a}_\parallel \cdot \nabla_\xi G d\sigma = \sum_{i=1}^3 \int_{\mathbf{d}_i} G(\xi, \eta) (\mathbf{a}_\parallel \cdot \nu_i) ds = (\mathbf{a} \times \mathbf{n}_t) \cdot \sum_{i=1}^3 \frac{\mathbf{d}_i}{\|\mathbf{d}_i\|} \int_{\mathbf{d}_i} G(\xi, \eta) ds. \tag{66}$$

The next step is to compute the line integral of the Laplacian fundamental solution  $\int_{\mathbf{d}_i} G(\xi, \eta) ds$ . Let  $r_k = \|\mathbf{e}_k\| = \|\mathbf{v}_{j_k} - \eta\|$  for  $k = 1, 2, 3$ , and let  $\mathbf{a} = \mathbf{e}_3$ ,  $\mathbf{b} = \mathbf{e}_2 - \mathbf{e}_3$  and define  $\gamma(t) = \mathbf{a} + t\mathbf{b}$  with  $t \in [0, 1]$ . We also have  $ds = \|\mathbf{b}\| dt$ . Therefore,

$$\int_{\mathbf{d}_i} G(\xi, \eta) ds = -\frac{\|\mathbf{b}\|}{4\pi} \int_0^1 \frac{dt}{\|\mathbf{a} + t\mathbf{b}\|}. \tag{67}$$

When  $A > 0$ , the following important integral formula holds:

$$\int \frac{dt}{\sqrt{At^2 + Bt + C}} = \frac{1}{\sqrt{A}} \log(2At + B + 2\sqrt{A}\sqrt{At^2 + Bt + C}) + \text{constant}, \quad (68)$$

where  $A = \|\mathbf{b}\|^2 = \|\mathbf{d}_1\|^2$ ,  $B = 2(\mathbf{a} \cdot \mathbf{b}) = 2(\mathbf{e}_2 \cdot \mathbf{d}_1) = \|\mathbf{e}_2\|^2 - \|\mathbf{e}_3\|^2 - \|\mathbf{d}_1\|^2$ ,  $C = \|\mathbf{e}_3\|^2$ . Then we have

$$\begin{aligned} \int_{\mathbf{d}_i} G(\xi, \eta) \, ds &= -\frac{1}{4\pi} \log \frac{2\|\mathbf{d}_1\|\|\mathbf{e}_2\| + 2\|\mathbf{d}_1\|^2 + (\|\mathbf{e}_2\|^2 - \|\mathbf{e}_3\|^2 - \|\mathbf{d}_1\|^2)}{2\|\mathbf{d}_1\|\|\mathbf{e}_3\| + (\|\mathbf{e}_2\|^2 - \|\mathbf{e}_3\|^2 - \|\mathbf{d}_1\|^2)} \\ &= -\frac{1}{4\pi} \log \frac{(\|\mathbf{e}_2\| + \|\mathbf{d}_1\|)^2 - \|\mathbf{e}_3\|^2}{\|\mathbf{e}_2\|^2 - (\|\mathbf{e}_3\| - \|\mathbf{d}_1\|)^2} \\ &= -\frac{1}{4\pi} \log \frac{\|\mathbf{e}_2\| + \|\mathbf{e}_3\| + \|\mathbf{d}_1\|}{\|\mathbf{e}_2\| + \|\mathbf{e}_3\| - \|\mathbf{d}_1\|}. \end{aligned} \quad (69)$$

Recall  $R_1 = \|\mathbf{e}_2\| + \|\mathbf{e}_3\|$ , we have

$$\int_{\mathbf{d}_i} G(\xi, \eta) \, ds = -\frac{1}{4\pi} \log \frac{R_1 + \|\mathbf{d}_1\|}{R_1 - \|\mathbf{d}_1\|}, \quad (70)$$

which is actually  $-C_1$  of Eq.(37). Moreover, we have

$$\int_{t_j} \mathbf{n}_t \cdot \nabla_{\xi} G(\xi, \eta) \, d\sigma_{\xi} = \omega_t. \quad (71)$$

Therefore,

$$\mathbf{a} \cdot \nabla \psi_t(\eta) = (\mathbf{a}_{\parallel} + (\mathbf{a} \cdot \mathbf{n}_t)\mathbf{n}_t) \cdot \int_{t_j} \nabla_{\xi} G(\xi, \eta) \, d\sigma_{\xi} = -(\mathbf{a} \times \mathbf{n}_t) \cdot \sum_{i=1}^3 C_i \mathbf{d}_i + (\mathbf{a} \cdot \mathbf{n}_t) \omega_t. \quad (72)$$

Using the property that  $(\mathbf{a} \times \mathbf{n}_t) \cdot \mathbf{b} = \mathbf{a} \cdot (\mathbf{n}_t \times \mathbf{b})$ , we obtain

$$\mathbf{a} \cdot \nabla \psi_t(\eta) = -\mathbf{a} \cdot \left( \mathbf{n}_t \times \sum_{i=1}^3 C_i \mathbf{d}_i - \omega_t \mathbf{n}_t \right) = \mathbf{a} \cdot (-P_t). \quad (73)$$

Since  $\mathbf{a}$  is arbitrary, we have

$$\boxed{\nabla \psi_t(\eta) = -P_t}. \quad (74)$$

**4. Derivation of  $\nabla \phi_{v_{j_1, t_j}}(\eta)$ .** The gradient of  $\phi_{v_{j_1, t_j}}(\eta)$  with respect to  $\eta$  can be directly obtained by differentiation as

$$\boxed{\nabla \phi_{v_{j_1, t_j}}(\eta) = \frac{1}{2A_t} (\mathbf{J}(\mathbf{Z}_1)^{\top} P_t + \mathbf{J}(P_t)^{\top} \mathbf{Z}_1)}. \quad (75)$$

We first compute the Jacobian matrix of  $\mathbf{Z}_1 = -\mathbf{e}_2 \times \mathbf{e}_3$ . Consider a perturbation  $\delta\eta$  to  $\eta$ . The corresponding variations in  $\mathbf{e}_2$  and  $\mathbf{e}_3$  are  $\delta\mathbf{e}_2 = -\delta\eta$  and  $\delta\mathbf{e}_3 = -\delta\eta$ . The variation of  $\mathbf{Z}_1$  is given by:

$$\delta\mathbf{Z}_1 = -\delta(\mathbf{e}_2 \times \mathbf{e}_3) = -(\delta\mathbf{e}_2) \times \mathbf{e}_3 - \mathbf{e}_2 \times (\delta\mathbf{e}_3) = (\delta\eta) \times \mathbf{e}_3 + \mathbf{e}_2 \times (\delta\eta) = (\mathbf{e}_2 - \mathbf{e}_3) \times \delta\eta. \quad (76)$$

Hence, the Jacobian matrix of  $\mathbf{Z}_1$  is

$$\boxed{\mathbf{J}(\mathbf{Z}_1) = [\mathbf{e}_2]_{\times} - [\mathbf{e}_3]_{\times} = [\mathbf{d}_1]_{\times}}, \quad (77)$$

where  $[\mathbf{u}]_{\times}$  denotes the skew-symmetric matrix such that, for any vector  $\mathbf{v}$ ,  $[\mathbf{u}]_{\times} \mathbf{v} = \mathbf{u} \times \mathbf{v}$ . An important property that will be utilized later is that  $[\mathbf{u}]_{\times}^{\top} = -[\mathbf{u}]_{\times}$ .

For  $\mathbf{J}(P_t)$ , we have

$$\mathbf{J}(P_t) = \sum_{i=1}^3 (\mathbf{n}_t \times \mathbf{d}_i) \nabla C_i^{\top} - \mathbf{n}_t \nabla \omega_t^{\top}. \quad (78)$$

We also have

$$\nabla C_i = \bar{C}_i (\bar{\mathbf{e}}_{i+1} + \bar{\mathbf{e}}_{i+2}). \quad (79)$$

Therefore,

$$\mathbf{J}(P_t) = [\mathbf{n}_t]_{\times} \begin{pmatrix} \mathbf{d}_1, \mathbf{d}_2, \mathbf{d}_3 \end{pmatrix}_{3 \times 3} \begin{pmatrix} \bar{C}_1 (\bar{\mathbf{e}}_2 + \bar{\mathbf{e}}_3)^{\top} \\ \bar{C}_2 (\bar{\mathbf{e}}_3 + \bar{\mathbf{e}}_1)^{\top} \\ \bar{C}_3 (\bar{\mathbf{e}}_1 + \bar{\mathbf{e}}_2)^{\top} \end{pmatrix}_{3 \times 3} - \mathbf{n}_t \nabla \omega_t^{\top}. \quad (80)$$

We also need to compute the derivative of  $\omega_t$  with respect to  $\eta$ , which can be obtained by taking the gradient of  $\psi_t(\eta)$ . Recall that

$$\psi_t(\eta) = - \sum_{i=1}^3 C_i (\mathbf{Z}_i \cdot \mathbf{n}_t) - \frac{3}{A_t} \omega_t \text{vol}_t, \quad (81)$$

and that its gradient with respect to  $\eta$  satisfies

$$\nabla \psi_t(\eta) = -P_t(\eta) = - \left( \mathbf{n}_t \times \sum_{i=1}^3 C_i \mathbf{d}_i - \omega_t \mathbf{n}_t \right). \quad (82)$$

Differentiating Eq. (81) with respect to  $\eta$  and obtain

$$\nabla \psi_t(\eta) = - \sum_{i=1}^3 \left[ (\mathbf{Z}_i \cdot \mathbf{n}_t) \nabla C_i + C_i \nabla (\mathbf{Z}_i \cdot \mathbf{n}_t) \right] - \frac{3}{A_t} \left( \text{vol}_t \nabla \omega_t + \omega_t \nabla \text{vol}_t \right). \quad (83)$$

The signed volume of the tetrahedron is  $\text{vol}_t = \frac{1}{3} A_t H_t$ . Consequently

$$\nabla \text{vol}_t = \frac{1}{3} A_t \nabla H_t = -\frac{1}{3} A_t \mathbf{n}_t. \quad (84)$$

Rearranging above formulation and get

$$\nabla \omega_t = -\frac{1}{H_t} \sum_{i=1}^3 (\mathbf{Z}_i \cdot \mathbf{n}_t) \bar{C}_i (\bar{\mathbf{e}}_{i+1} + \bar{\mathbf{e}}_{i+2}), \quad (85)$$

where  $H_t$  is the height of  $\eta$  toward  $t$ , which can also computed as  $H_t = \mathbf{e}_1 \cdot \mathbf{n}_t$ .

**5. Derivation of  $H_\eta \psi_t(\eta)$ .** The Hessian  $\psi_t(\eta)$  can be obtained by

$$H_\eta \psi_t(\eta) = -\mathbf{J}(P_t), \quad (86)$$

which have already been calculated in Eq. (80).

**6. Derivation of  $H_\eta \phi_{v_{j_1}, t_j}(\eta)$ .** Since  $\mathbf{J}(\mathbf{Z}_1)^{\top} = [\mathbf{d}_1]_{\times}^{\top} = -[\mathbf{d}_1]_{\times}$ , we have

$$H_\eta \phi_{v_{j_1}, t_j}(\eta) = \frac{1}{2A_t} (-[\mathbf{d}_1]_{\times} \mathbf{J}(P_t) + \mathbf{J}(\mathbf{J}(P_t)^{\top} \mathbf{Z}_1)). \quad (87)$$

We now focus on the calculation of  $\mathbf{J}(\mathbf{J}(P_t)^{\top} \mathbf{Z}_1)$  as

$$\mathbf{J}(\mathbf{J}(P_t)^{\top} \mathbf{Z}_1) = \mathbf{J}(P_t)^{\top} \mathbf{J}(\mathbf{Z}_1) + \sum_{k=1}^3 [\mathbf{Z}_1]_k \mathbf{J}([\mathbf{J}(P_t)^{\top}]_{:,k}). \quad (88)$$

We write

$$\mathbf{Q} = \mathbf{J}(P_t)^\top = -\mathbf{M}\mathbf{D}[\mathbf{n}_t]_\times - \nabla\omega_t \mathbf{n}_t^\top, \quad \mathbf{M} = \begin{pmatrix} \bar{C}_1(\bar{\mathbf{e}}_2 + \bar{\mathbf{e}}_3)^\top \\ \bar{C}_2(\bar{\mathbf{e}}_3 + \bar{\mathbf{e}}_1)^\top \\ \bar{C}_3(\bar{\mathbf{e}}_1 + \bar{\mathbf{e}}_2)^\top \end{pmatrix}_{3 \times 3}^\top, \quad \mathbf{D} = (\mathbf{d}_1, \mathbf{d}_2, \mathbf{d}_3)_{3 \times 3}^\top. \quad (89)$$

Moreover,

$$[\mathbf{Q}]_{:,k} = -[\mathbf{M}\mathbf{D}[\mathbf{n}_t]_\times]_{:,k} - [\nabla\omega_t \mathbf{n}_t^\top]_{:,k} = -\mathbf{M}\mathbf{u}_k - [\mathbf{n}_t]_k \nabla\omega_t = -\sum_{l=1}^3 [\mathbf{u}_k]_l \mathbf{m}_l - [\mathbf{n}_t]_k \nabla\omega_t, \quad (90)$$

where  $\mathbf{u}_k = [\mathbf{D}[\mathbf{n}_t]_\times]_{:,k}$  does not depend on  $\eta$ , and  $\mathbf{m}_l = \bar{C}_l(\bar{\mathbf{e}}_{l+1} + \bar{\mathbf{e}}_{l+2})$ . Therefore,

$$\mathbf{J}([\mathbf{Q}]_{:,k}) = -\sum_{l=1}^3 [\mathbf{u}_k]_l \mathbf{J}(\mathbf{m}_l) - [\mathbf{n}_t]_k \mathbf{H}_{\omega_t}, \quad (91)$$

where  $\mathbf{H}_{\omega_t}$  is the Hessian matrix of  $\omega_t$  with respect to  $\eta$ . Therefore,

$$\begin{aligned} \mathbf{J}(\mathbf{J}(P_t)^\top \mathbf{Z}_1) &= \mathbf{J}(P_t)^\top ([\mathbf{e}_2]_\times - [\mathbf{e}_3]_\times) - \sum_{l=1}^3 \left( \sum_{k=1}^3 [\mathbf{Z}_1]_k [\mathbf{u}_k]_l \right) \mathbf{J}(\mathbf{m}_l) - \left( \sum_{k=1}^3 [\mathbf{Z}_1]_k [\mathbf{n}_t]_k \right) \mathbf{H}_{\omega_t} \\ &= \mathbf{J}(P_t)^\top ([\mathbf{e}_2]_\times - [\mathbf{e}_3]_\times) - \sum_{l=1}^3 [\mathbf{U}\mathbf{Z}_1]_l \mathbf{J}(\mathbf{m}_l) - (\mathbf{Z}_1 \cdot \mathbf{n}_t) \mathbf{H}_{\omega_t}, \end{aligned} \quad (92)$$

where  $\mathbf{U} = \mathbf{D}[\mathbf{n}_t]_\times$ . For other values, we have

$$\begin{aligned} \mathbf{J}(\mathbf{m}_l) &= \nabla \bar{C}_l(\bar{\mathbf{e}}_{l+1} + \bar{\mathbf{e}}_{l+2})^\top + \bar{C}_l(\mathbf{J}(\bar{\mathbf{e}}_{l+1}) + \mathbf{J}(\bar{\mathbf{e}}_{l+2})), \\ \nabla \bar{C}_l &= \frac{R_l}{\pi(R_l^2 - \|\mathbf{d}_l\|^2)^2} (\bar{\mathbf{e}}_{l+1} + \bar{\mathbf{e}}_{l+2}), \\ \mathbf{J}(\bar{\mathbf{e}}_i) &= -\frac{1}{\|\mathbf{e}_i\|} (\mathbf{I} - \bar{\mathbf{e}}_i \bar{\mathbf{e}}_i^\top). \end{aligned} \quad (93)$$

We then compute the Hessian of  $\omega_t$ . Denoting  $\mathbf{S} = -\sum_{i=1}^3 (\mathbf{Z}_i \cdot \mathbf{n}_t) \bar{C}_i(\bar{\mathbf{e}}_{i+1} + \bar{\mathbf{e}}_{i+2})$ , we have

$$\mathbf{H}_{\omega_t} = \mathbf{J}\left(\frac{1}{H_t} \mathbf{S}\right) = \frac{1}{H_t^2} \mathbf{S} \mathbf{n}_t^\top + \frac{1}{H_t} \mathbf{J}(\mathbf{S}). \quad (94)$$

We write  $\mathbf{S} = \sum_i a_i \mathbf{u}_i$ , where  $a_i = -(\mathbf{Z}_i \cdot \mathbf{n}_t) \bar{C}_i$ ,  $\mathbf{u}_i = \bar{\mathbf{e}}_{i+1} + \bar{\mathbf{e}}_{i+2}$ . Then,

$$\mathbf{J}(\mathbf{S}) = \sum_{i=1}^3 \mathbf{J}(a_i \mathbf{u}_i) = \mathbf{u}_i (\nabla a_i)^\top + a_i \mathbf{J}(\mathbf{u}_i). \quad (95)$$

Recall  $a_i = s_i \bar{C}_i$  with  $s_i = -\mathbf{Z}_i \cdot \mathbf{n}_t$ . Thus

$$\nabla a_i = \bar{C}_i \nabla s_i + s_i \nabla \bar{C}_i. \quad (96)$$

$\nabla s_i$  can be obtained by

$$\nabla s_i = -\nabla(\mathbf{Z}_i \cdot \mathbf{n}_t) = -\mathbf{J}(\mathbf{Z}_i)^\top \mathbf{n}_t = -\mathbf{n}_t \times \mathbf{d}_i. \quad (97)$$

Moreover, we have already computed that  $\nabla \bar{C}_i = \frac{R_i}{\pi(R_i^2 - \|\mathbf{d}_i\|^2)^2} \mathbf{u}_i$ . Define  $\gamma_i = \frac{R_i}{\pi(R_i^2 - \|\mathbf{d}_i\|^2)^2}$ , we have

$$\nabla a_i = -\bar{C}_i(\mathbf{n}_t \times \mathbf{d}_i) + s_i \gamma_i \mathbf{u}_i. \quad (98)$$

Since  $\mathbf{u}_i = \bar{\mathbf{e}}_{i+1} + \bar{\mathbf{e}}_{i+2}$ , we have

$$\mathbf{J}(\mathbf{u}_i) = -\frac{1}{\|\mathbf{e}_{i+1}\|} (\mathbf{I} - \bar{\mathbf{e}}_{i+1} \bar{\mathbf{e}}_{i+1}^\top) - \frac{1}{\|\mathbf{e}_{i+2}\|} (\mathbf{I} - \bar{\mathbf{e}}_{i+2} \bar{\mathbf{e}}_{i+2}^\top). \quad (99)$$

Therefore,

$$\mathbf{H}_{\omega_t} = \frac{1}{H_t^2} \mathbf{S} \mathbf{n}_t^\top + \frac{1}{H_t} \sum_{i=1}^3 [\mathbf{u}_i (\nabla a_i)^\top + a_i \mathbf{J}(\mathbf{u}_i)], \quad (100)$$

where

$$\mathbf{u}_i = \bar{\mathbf{e}}_{i+1} + \bar{\mathbf{e}}_{i+2}, \quad a_i = s_i \bar{C}_i, \quad s_i = -(\mathbf{Z}_i \cdot \mathbf{n}_t), \quad \nabla a_i = -\bar{C}_i (\mathbf{n}_t \times \mathbf{d}_i) + s_i \gamma_i \mathbf{u}_i, \quad \gamma_i = \frac{R_i}{\pi(R_i^2 - \|\mathbf{d}_i\|^2)^2}. \quad (101)$$

## C Supplementary Information for Experiments

### C.1 Anisotropic Matrices

Here, we provide some anisotropic matrices used in 2D deformation experiments. Note that  $\mathcal{A}(\theta, 1, \lambda) = \mathcal{A}(\theta + \frac{\pi}{2}, \lambda, 1)$ , so all rotation angles listed in the table are less than  $\frac{\pi}{2}$ .

$\theta$	$(\lambda_1, \lambda_2) = (1.0, 2.0)$	$(\lambda_1, \lambda_2) = (1.0, 4.0)$	$(\lambda_1, \lambda_2) = (2.0, 1.0)$	$(\lambda_1, \lambda_2) = (4.0, 1.0)$
0	$\begin{pmatrix} 1.0 & 0 \\ 0 & 2.0 \end{pmatrix}$	$\begin{pmatrix} 1.0 & 0 \\ 0 & 4.0 \end{pmatrix}$	$\begin{pmatrix} 2.0 & 0 \\ 0 & 1.0 \end{pmatrix}$	$\begin{pmatrix} 4.0 & 0 \\ 0 & 1.0 \end{pmatrix}$
$\pi/6$	$\begin{pmatrix} 1.25 & -0.4330127 \\ -0.4330127 & 1.75 \end{pmatrix}$	$\begin{pmatrix} 1.75 & -1.2990381 \\ -1.2990381 & 3.25 \end{pmatrix}$	$\begin{pmatrix} 1.75 & 0.4330127 \\ 0.4330127 & 1.25 \end{pmatrix}$	$\begin{pmatrix} 3.25 & 1.2990381 \\ 1.2990381 & 1.75 \end{pmatrix}$
$\pi/4$	$\begin{pmatrix} 1.5 & -0.5 \\ -0.5 & 1.5 \end{pmatrix}$	$\begin{pmatrix} 2.5 & -1.5 \\ -1.5 & 2.5 \end{pmatrix}$	$\begin{pmatrix} 1.5 & 0.5 \\ 0.5 & 1.5 \end{pmatrix}$	$\begin{pmatrix} 2.5 & 1.5 \\ 1.5 & 2.5 \end{pmatrix}$
$\pi/3$	$\begin{pmatrix} 1.75 & -0.4330127 \\ -0.4330127 & 1.25 \end{pmatrix}$	$\begin{pmatrix} 3.25 & -1.2990381 \\ -1.2990381 & 1.75 \end{pmatrix}$	$\begin{pmatrix} 1.25 & 0.4330127 \\ 0.4330127 & 1.75 \end{pmatrix}$	$\begin{pmatrix} 1.75 & 1.2990381 \\ 1.2990381 & 3.25 \end{pmatrix}$

### C.2 Computation of distortion

We compute the isometric distortion  $E_{\text{iso}}$ , conformal distortion  $E_{\text{conf}}$  and area distortion  $E_{\text{area}}$  as follows:

$$E_{\text{iso}} = (\sigma_1 - 1)^2 + (\sigma_2 - 1)^2, \quad (102)$$

where  $\sigma_1$  and  $\sigma_2$  are the two singular values of the Jacobian matrix of the deformation map. The conformal distortion evaluates the deviation from angle preservation and is expressed as

$$E_{\text{conf}} = \frac{\sigma_1}{\sigma_2} + \frac{\sigma_2}{\sigma_1} - 2, \quad (103)$$

which vanishes if and only if  $\sigma_1 = \sigma_2$ . Finally, the area distortion quantifies the deviation from unit area scaling and is given by

$$E_{\text{area}} = |\sigma_1 \sigma_2 - 1|. \quad (104)$$

The metrics are computed as the average over all pixels in the input image.

## References

- Mirela Ben-Chen, Ofir Weber, and Craig Gotsman. 2009. Variational harmonic maps for space deformation. *ACM Transactions on Graphics* 28, 3 (2009), 34.
- Yaron Lipman and David Levin. 2009. Derivation and analysis of Green coordinates. *Computational Methods and Function Theory* 10, 1 (2009), 167.
- Yaron Lipman, David Levin, and Daniel Cohen-Or. 2008. Green coordinates. *ACM Transactions on Graphics* 27, 3 (2008), 78.
- Élie Michel, Alec Jacobson, Siddhartha Chaudhuri, and Jean-Marc Thiery. 2025. Variational Green and Biharmonic Coordinates for 2D Polynomial Cages. *ACM Trans. Graph.* 44, 4 (2025), 76:1–76:20.
- Masataka Urago. 2000. Analytical Integrals of Fundamental Solution of Three-Dimensional Laplace Equation and Their Gradients. *Transactions of the Japan Society of Mechanical Engineers Series A* 66, 642 (2000), 254–260. in Japanese.